Computer Modeling in Engineering & Sciences

Tech Science Press

Doi:10.32604/cmes.2025.059948

ARTICLE

A Study of the 1 + 2 Partitioning Scheme of Fibrous Unitcell under Reduced-Order Homogenization Method with Analytical Influence Functions

Shanqiao Huang[1] **and Zifeng Yuan**[1,2,*]

[1]HEDPS, Center for Applied Physics and Technology (CAPT), Department of Mechanics and Engineering Science, College of Engineering, Peking University, Beijing, 100871, China

[2]State Key Laboratory for Turbulence and Complex Systems, Peking University, Beijing, 100871, China

*Corresponding Author: Zifeng Yuan. Email: yuanzifeng@pku.edu.cn

Received: 21 October 2024; Accepted: 21 January 2025; Published: 03 March 2025

ABSTRACT: The multiscale computational method with asymptotic analysis and reduced-order homogenization (ROH) gives a practical numerical solution for engineering problems, especially composite materials. Under the ROH framework, a partition-based unitcell structure at the mesoscale is utilized to give a mechanical state at the macro-scale quadrature point with pre-evaluated influence functions. In the past, the "1-phase, 1-partition" rule was usually adopted in numerical analysis, where one constituent phase at the mesoscale formed one partition. The numerical cost then is significantly reduced by introducing an assumption that the mechanical responses are the same all the time at the same constituent, while it also introduces numerical inaccuracy. This study proposes a new partitioning method for fibrous unitcells under a reduced-order homogenization methodology. In this method, the fiber phase remains 1 partition, but the matrix phase is divided into 2 partitions, which refers to the "1 + 2" partitioning scheme. Analytical elastic influence functions are derived by introducing the elastic strain energy equivalence (Hill-Mandel condition). This research also obtains the analytical eigenstrain influence functions by alleviating the so-called "inclusion-locking" phenomenon. In addition, a numerical approach to minimize the error of strain energy density is introduced to determine the partitioning of the matrix phase. Several numerical examples are presented to compare the differences among direct numerical simulation (DNS), "1 + 1", and "1 + 2" partitioning schemes. The numerical simulations show improved numerical accuracy by the "1 + 2" partitioning scheme.

KEYWORDS: Multiscale; reduced-order homogenization; influence tensors; unitcell; fibrous composite material

1 Introduction

Fibrous composite materials with the advantages of high specific strength, specific stiffness, and corrosion resistance are widely used in many advanced manufacturing sectors, and that leads to the demand for high-fidelity evaluation of mechanical properties of the composite structures [1–3]. However, the overall mechanical response of composite materials is complicated because of the large gap between the mechanical properties of each constituent, especially when the nonlinearities are considered. The various mesoscale geometric structures of fibrous composite materials and loading patterns also lead to different types of material failure, such as breakage of fibers, debonding of fiber/matrix interface, or delamination of plies. Therefore, developing an efficient framework for the constitutive model of composite materials with comprehensive consideration of various nonlinear material behaviors is important, and a series of research has been conducted in this area. Firstly, various homogenized anisotropic damage models of the composite material were proposed [4–6] and applied in engineering. Meanwhile, based on the high-resolution modeling,

many investigations were conducted to capture the failure mechanism on the mesoscale [7–9]. In these homogenized damage models, the loss of microscale information usually leads to a loss of accuracy and generalizability; the increasing complexity of the homogenized model also requires extensive calibration. On the other hand, the orders of magnitude gap between the characteristic length of the mesoscale model and composite structure gives rise to unacceptable computation costs. Therefore, the so-called multiscale method based on continuum mechanics, also labeled as an upscaling method, has been developed rapidly to balance fidelity and computation efficiency. A series of works on direct multiscale methods, such as the multilevel finite element (FE^2) approach [10], the first-order nonlinear computational homogenization methods [11], and the higher-order homogenization [12], have made significant improvements in addressing this dilemma of scales. However, the number of unknown variables within a single unitcell is still too large for engineering applications. This required further model simplification or model reduction at the mesoscale, leading to the proposal of reduced-order models for heterogeneous continua.

Transformation field analysis (TFA) is a typical reduced model proposed by Dvorak for the analysis of elastic composite [13] and then extended for the inelastic cases [14]. The scale transitions of strain and stress in heterogeneous structures were expressed explicitly by this approach, where plastic strain and thermal expansion were treated as eigenstrain. In TFA, the transformation influence functions and concentration factors are precomputed based on the mechanical parameters of different phases and the geometric structure of the composite. The number of variables was reduced significantly due to the assumption of piecewise uniform fields. Therefore, this approach was utilized and developed for the analyses of composite structures by many scholars over the past three decades [15–17]. However, some deficiencies of classical TFA were recognized in practice. First, the prediction of macroscopic stress is usually too stiff due to the assumption of piecewise uniform plastic strain [18,19]. In addition, expectedly, the accuracy of the two-phase system in inelastic analysis is unsatisfactory when following the principle of so-called "1-phase-1-partition". That leads to the finer division of each individual phase, in other words, a larger number of internal variables in overall constitutive relations [20]. Instead of finer division in the space domain of each phase, decomposing the plastic strain into a finite combination set of plastic modes, the so-called nonuniform transformation field analysis (NTFA) [21,22], is another option for reaching higher precision. However, the extra work for calibrating empirical laws and extensive exploration of the deformation space under plastic deformation can counteract the advantage of NTFA on computational efficiency.

Liu et al. proposed the self-consistent clustering analysis (SCA) method [23] to overcome the limitations of TFA and its derivatives. In the SCA method, the constituents of composites are divided into a specific number of subdomains by k-means clustering based on the linear response of the unitcell, while a self-consistent implicit scheme is adopted for updating the macroscopic tangent modulus. Due to the high computation efficiency on heterogeneous materials, SCA is absorbing great attention and has been developed for a series of inelastic response analyses, including elastoplasticity, strain-softening, fatigue-strength prediction, and so on [24–27]. The extensions of SCA were also proposed for local mechanical analysis of composites and simplification of implementation [28,29]. In addition, k-means clustering is also combined with other reduced-order methods, such as NTFA [30,31]. On the other hand, other cluster-discretization methods, including the virtual clustering analysis (VCA) [32] and the FEM clustering analysis (FCA) [33], were developed as optional solutions of interaction tensors. Naturally, these cluster-discretization methods have been utilized for the research of machine learning-based multiscale modeling, especially in the generation of databases. SCA was applied for data mining and uncertainty analysis in a unified data-driven computational framework to design and model materials and structures [34]. A reduced-order model involving three scales was developed for woven composites using a data-driven SCA × SCA multiscale simulation framework [35]. Li et al. built a framework in which cluster-discretization methods are applied to develop a material behavior

database for training neural networks, including feed-forward neural networks (FFNN) and convolutional neural networks (CNN) [36]. They presented its application on multiscale topology optimization.

Other machine learning-based multiscale techniques have also been developed as an important direction of model reduction. Zhang et al. [37] developed a reduced-order model of the hierarchical deep-learning neural networks (HiDeNN) based on a tensor decomposition (TD). A reduced-order machine learning finite element method based on proper generalized decomposition (PGD) reduced HiDeNN presents a good performance in the multiscale analysis of composite materials, topology optimization, and additive manufacturing [38]. Fish et al. [39,40] proposed a data-physics-driven reduced-order homogenization (dpROH) approach, which significantly improves the accuracy of physics-based reduced-order homogenization (pROH) by combining data generated from high-fidelity models with Bayesian inference. The artificial neural network (ANN) and deep material network (DMN) were also applied to homogenize the nonlinear mechanical properties of heterogeneous materials [41,42]. Masrouri et al. [43] utilized generative AI to predict the stress distribution of bicontinuous composites with complex irregular distribution.

The motivation of the present work is to develop a reduced-order homogenization (ROH) multiscale method [44–47] for fibrous composite material, in which the overestimation of strength due to "1-phase-1-partition" is improved while no extra internal variables of the constitutive model of each phase are introduced; in addition, simple and explicit partitioning of the subdomains of constituents is preferred over to the complicated and implicit partitioning of cluster-discretization methods. Therefore, a framework of constitutive model based on the ROH method is proposed, in which an adaptive method for partitioning the matrix phase is involved. This model can capture the stress concentration on the mesoscale and predict the overall response of fibrous composite with better precision since the matrix phase is divided into inner and outer matrix partitions with an independent nonlinear evolution process. The volume fraction of the inner matrix partition is predicted by a numerical calculation method, whose object function targets the minimization of error in strain energy density compared to the results from a modified Eshelby method [48–51]. In addition, the influence functions of elastic strain and eigenstrain are calculated analytically so that the offline computation is simplified drastically. In this manuscript, the framework of reduced-order homogenization is briefly introduced in Section 2; the mathematical manipulation of the analytical solution of influence functions for 1 + 2 partitions is presented in Section 3, along with the numerical calculation method for partitioning of the matrix phase; the numerical results for the verification of new model under different volume fractions of fiber are exhibited in Section 4; finally, the discussion of the numerical results and the corresponding conclusions are provided in Sections 5 and 6, respectively.

2 Reduced-Order Homogenization

The multiscale computational homogenization method based on the unitcell discretized by finite elements is usually computationally prohibitive for general macroscopic structures. It requires averaging and homogenization procedures over a converged unitcell problem at every macroscopic integration point during each Newton-Raphson iteration. In addition, the unitcell problem involving material nonlinearities needs to be solved using a Newton-Raphson iterative method. Model reduction technique is necessary to reduce the degrees of freedom by applying a specific distribution of mechanical response over phases at the mesoscale. The reduced-order homogenization (ROH) approach is a typical multiscale method with low computational cost, adopting a piecewise constant approximation of mechanical quantities over each partition.

In addition, the concept of eigenstrain is introduced to consider the material nonlinear response that

$$\boldsymbol{\mu}^{(\alpha)} = \boldsymbol{\varepsilon}^{(\alpha)} - \mathbb{M}^{(\alpha)} : \boldsymbol{\sigma}^{(\alpha)}, \quad \alpha = 1, 2, \cdots, M \tag{1}$$

where M is the number of partitions, $\mathbb{M}^{(\alpha)} = [M_{ijkl}^{(\alpha)}]$ is the compliance coefficient tensor for the α-th partition. The reduced-order homogenization method assumes that the material response, including the strain, stress, and state variables, keeps the same within one partition all the time and thus introduces the following reduced equilibrium equations (see Chapter 4 of the book [52]):

$$\boldsymbol{\varepsilon}^{(\beta)} - \sum_{\alpha=1}^{M} \mathbb{P}^{(\beta\alpha)} : \boldsymbol{\mu}^{(\alpha)} = \mathbb{E}^{(\beta)} : \boldsymbol{\varepsilon}^{\mathrm{C}},\ \beta = 1, 2, \cdots, M \tag{2}$$

where $\mathbb{E}^{(\alpha)} = [E_{ij}^{kl(\alpha)}], \alpha = 1, 2, \cdots, M$ are the *elastic strain influence functions* for the α-th partition, and $\mathbb{P}^{(\beta\alpha)} = [P_{ij}^{kl(\beta\alpha)}], \alpha, \beta = 1, 2, \cdots, M$ are the *eigenstrain influence functions* measuring the interaction between the α-th and β-th partitions, and $\boldsymbol{\varepsilon}^{\mathrm{C}}$ is the macroscopic strain.

The elastic strain influence functions satisfy the following two constraints:

$$\sum_{\alpha=1}^{M} c_\alpha \mathbb{E}^{(\alpha)} = \mathbb{I} \tag{3}$$

$$\sum_{\alpha=1}^{M} c_\alpha \mathbb{L}^{(\alpha)} : \mathbb{E}^{(\alpha)} = \mathbb{L}^{\mathrm{C}} \tag{4}$$

with c_α the volume fraction of α-th partition, and $\mathbb{L}^{\mathrm{C}} = [L_{ijkl}^{\mathrm{C}}]$ the linear homogenized elastic stiffness tensor. By (3) and (4), it can derive analytical results for the elastic strain influence functions when $M = 2$ with a given $\mathbb{L}^{\mathrm{C}}$ (Chapter 4 of the book [52]):

$$\mathbb{E}^{(1)} = \frac{1}{c_1}\left(\mathbb{L}^{(1)} - \mathbb{L}^{(2)}\right)^{-1} : \left(\mathbb{L}^{\mathrm{C}} - \mathbb{L}^{(2)}\right) \tag{5}$$

$$\mathbb{E}^{(2)} = \frac{1}{c_2}\left(\mathbb{L}^{(2)} - \mathbb{L}^{(1)}\right)^{-1} : \left(\mathbb{L}^{\mathrm{C}} - \mathbb{L}^{(1)}\right) \tag{6}$$

A two-partition unitcell model can be used for a general inclusion-matrix heterogeneous material under the assumption that each phase material always keeps the same response. Thus, it significantly reduces computational costs compared to the so-called direct-homogenization.

3 Fibrous Unitcell with 1 + 2 Partitions

The "1-phase-1-partition" reduced-order homogenization (ROH) method significantly decreases computational cost. However, under general multi-axial deformation, the distribution of material status within one phase is not uniform, which can give a stiffer material response than the direct-homogenization method due to the over-constraint of the material points. This study takes a fibrous unitcell as an example, as depicted in Fig. 1, and the matrix phase is partitioned into the inner and outer partitions. It visualizes the stress distribution under different loading modes, including uniaxial tension in longitudinal (Fig. 2a,b) and transverse (Fig. 2e,f) directions, shear in the longitudinal-transverse plane (Fig. 2c,d) and transverse plane (Fig. 2g,h). These numerical results show different stress magnitudes between the inner and outer partitions at the matrix phase.

This study uses the ROH method for the fibrous unitcell with two partitions at the matrix phase. We define this partition as a "1 + 2" partition. Due to the transverse isotropy symmetry of fibrous composite material, this study divided the matrix phase into the inner and outer partitions, as depicted in Fig. 1c,d, respectively. In the rest of the paper, the properties and status associated with the fiber phase, matrix phase, inner matrix partition, outer matrix partition, unitcell (mesoscale), and coarse (macroscopic) scale are

denoted as $\square^{\mathrm{f}}$, $\square^{\mathrm{m}}$, $\square^{\mathrm{a}}$, $\square^{\mathrm{b}}$, $\square^{\mathrm{uc}}$, and $\square^{\mathrm{c}}$, respectively. This study aims to obtain analytical formulations for the elastic strain and eigenstrain influence functions of the "1 + 2" partitions.

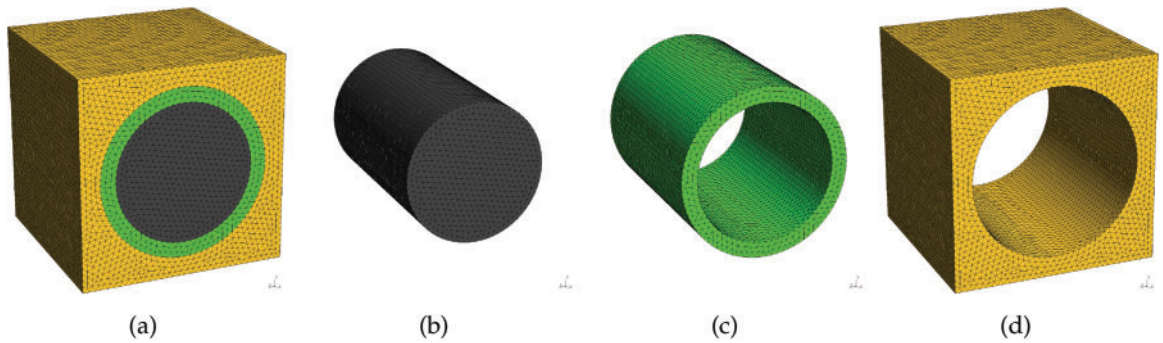

Figure 1: A sketch of a three-partition fibrous unitcell with finite element discretization: (a) fibrous unitcell; (b) fiber phase; (c) inner matrix partition; and (d) outer matrix partition

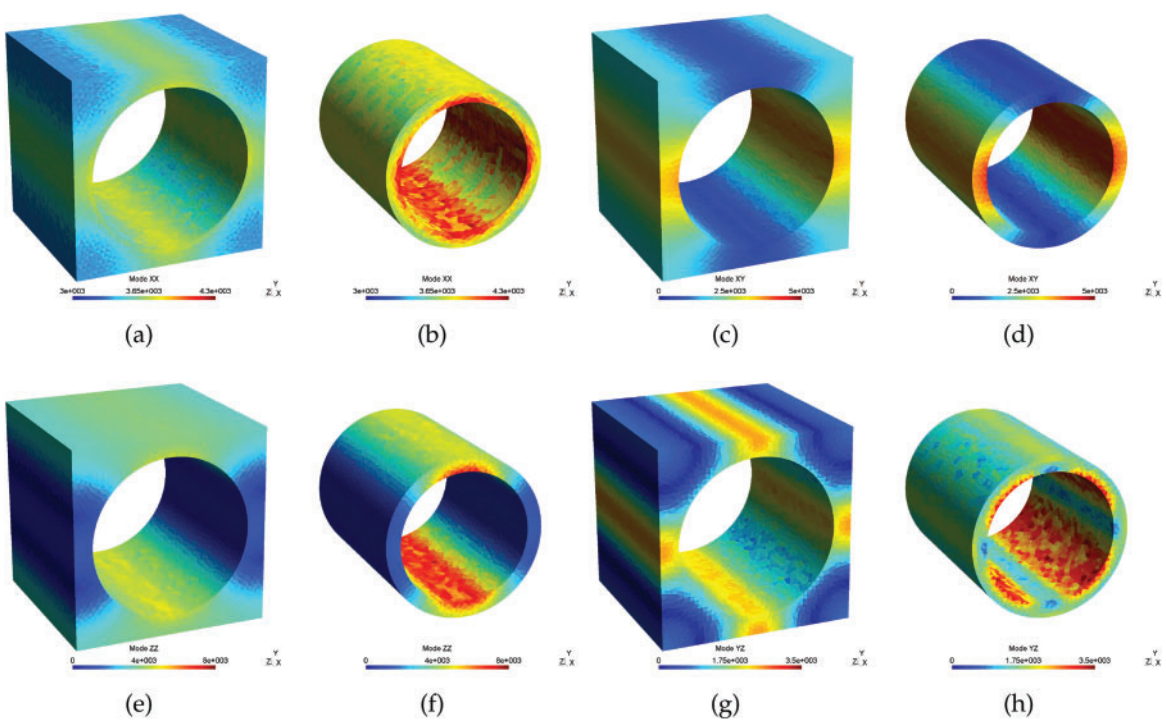

Figure 2: A sketch of von Mises stress of 1st and 2nd matrix partition under different loading modes: (a and b) uniaxial tension along the longitudinal direction; (c and d) simple shear at the longitudinal-transverse plane; (e and f) uniaxial tension along the transverse direction; and (g and h) simple shear at the transverse plane

3.1 Elastic Strain Influence Functions

From the point of view of macroscopic elastic strain energy density, the following can be obtained:

$$\mathcal{U}^{\mathrm{c}} = \frac{1}{2}\boldsymbol{\sigma}^{\mathrm{c}} : \boldsymbol{\varepsilon}^{\mathrm{c}} = \frac{1}{2}\boldsymbol{\varepsilon}^{\mathrm{c}} : \mathbb{L}^{\mathrm{c}} : \boldsymbol{\varepsilon}^{\mathrm{c}} \tag{7}$$

On the other hand, the mesoscale partitions give the elastic strain energy density that

$$\mathcal{U}^{\mathrm{uc}} = \frac{1}{2}c_{\mathrm{f}}\boldsymbol{\sigma}^{\mathrm{f}} : \boldsymbol{\varepsilon}^{\mathrm{f}} + \frac{1}{2}c_{\mathrm{a}}\boldsymbol{\sigma}^{\mathrm{a}} : \boldsymbol{\varepsilon}^{\mathrm{a}} + \frac{1}{2}c_{\mathrm{b}}\boldsymbol{\sigma}^{\mathrm{b}} : \boldsymbol{\varepsilon}^{\mathrm{b}} = \frac{1}{2}c_{\mathrm{f}}\boldsymbol{\varepsilon}^{\mathrm{f}} : \mathbb{L}^{\mathrm{f}} : \boldsymbol{\varepsilon}^{\mathrm{f}} + \frac{1}{2}c_{\mathrm{a}}\boldsymbol{\varepsilon}^{\mathrm{a}} : \mathbb{L}^{\mathrm{m}} : \boldsymbol{\varepsilon}^{\mathrm{a}} + \frac{1}{2}c_{\mathrm{b}}\boldsymbol{\varepsilon}^{\mathrm{b}} : \mathbb{L}^{\mathrm{m}} : \boldsymbol{\varepsilon}^{\mathrm{b}} \tag{8}$$

Under elastic response, the averaged strains at partitions are given as follows:

$$\boldsymbol{\varepsilon}^{\mathrm{f}} = \mathbb{E}^{\mathrm{f}} : \boldsymbol{\varepsilon}^{\mathrm{c}}, \boldsymbol{\varepsilon}^{\mathrm{a}} = \mathbb{E}^{\mathrm{a}} : \boldsymbol{\varepsilon}^{\mathrm{c}}, \boldsymbol{\varepsilon}^{\mathrm{b}} = \mathbb{E}^{\mathrm{b}} : \boldsymbol{\varepsilon}^{\mathrm{c}} \tag{9}$$

Substituting (9) into (8) yields

$$\mathcal{U}^{\mathrm{uc}} = \frac{1}{2}c_{\mathrm{f}}\boldsymbol{\varepsilon}^{\mathrm{c}} : \mathbb{E}^{\mathrm{f}} : \mathbb{L}^{\mathrm{f}} : \mathbb{E}^{\mathrm{f}} : \boldsymbol{\varepsilon}^{\mathrm{c}} + \frac{1}{2}c_{\mathrm{a}}\boldsymbol{\varepsilon}^{\mathrm{c}} : \mathbb{E}^{\mathrm{a}} : \mathbb{L}^{\mathrm{m}} : \mathbb{E}^{\mathrm{a}} : \boldsymbol{\varepsilon}^{\mathrm{c}} + \frac{1}{2}c_{\mathrm{b}}\boldsymbol{\varepsilon}^{\mathrm{c}} : \mathbb{E}^{\mathrm{b}} : \mathbb{L}^{\mathrm{m}} : \mathbb{E}^{\mathrm{b}} : \boldsymbol{\varepsilon}^{\mathrm{c}} \tag{10}$$

Comparing (7) and (10) and asking for $\mathcal{U}^{\mathrm{c}} = \mathcal{U}^{\mathrm{uc}}$ holds for arbitrary $\varepsilon^{\mathrm{c}}_{ij}$ yield

$$c_{\mathrm{f}}\mathbb{E}^{\mathrm{f}} : \mathbb{L}^{\mathrm{f}} : \mathbb{E}^{\mathrm{f}} + c_{\mathrm{a}}\mathbb{E}^{\mathrm{a}} : \mathbb{L}^{\mathrm{m}} : \mathbb{E}^{\mathrm{a}} + c_{\mathrm{b}}\mathbb{E}^{\mathrm{b}} : \mathbb{L}^{\mathrm{m}} : \mathbb{E}^{\mathrm{b}} = \mathbb{L}^{\mathrm{c}} \tag{11}$$

In addition, recall the equations for the elastic strain influence functions (3) and (4) for the fibrous unitcell that

$$c_{\mathrm{f}}\mathbb{E}^{\mathrm{f}} + c_{\mathrm{a}}\mathbb{E}^{\mathrm{a}} + c_{\mathrm{b}}\mathbb{E}^{\mathrm{b}} = \mathbb{I} \qquad \Rightarrow c_{\mathrm{f}}\mathbb{E}^{\mathrm{f}} + c_{\mathrm{m}}\left(\frac{c_{\mathrm{a}}}{c_{\mathrm{m}}}\mathbb{E}^{\mathrm{a}} + \frac{c_{\mathrm{b}}}{c_{\mathrm{m}}}\mathbb{E}^{\mathrm{b}}\right) = \mathbb{I} \tag{12}$$

$$c_{\mathrm{f}}\mathbb{L}^{\mathrm{f}} : \mathbb{E}^{\mathrm{f}} + c_{\mathrm{a}}\mathbb{L}^{\mathrm{m}} : \mathbb{E}^{\mathrm{a}} + c_{\mathrm{b}}\mathbb{L}^{\mathrm{m}} : \mathbb{E}^{\mathrm{b}} = \mathbb{L}^{\mathrm{c}} \quad \Rightarrow c_{\mathrm{f}}\mathbb{L}^{\mathrm{f}} : \mathbb{E}^{\mathrm{f}} + c_{\mathrm{m}}\mathbb{L}^{\mathrm{m}} : \left(\frac{c_{\mathrm{a}}}{c_{\mathrm{m}}}\mathbb{E}^{\mathrm{a}} + \frac{c_{\mathrm{b}}}{c_{\mathrm{m}}}\mathbb{E}^{\mathrm{b}}\right) = \mathbb{L}^{\mathrm{c}} \tag{13}$$

where $c_{\mathrm{m}} \equiv c_{\mathrm{a}} + c_{\mathrm{b}} = 1 - c_{\mathrm{f}}$ is the volume fraction of the matrix phase. Thus, a nonlinear system is obtained regarding the elastic strain influence functions $\mathbb{E}^{\dagger}, \dagger = \mathtt{f}, \mathtt{a}, \mathtt{b}$. First, from (12) and (13), the following can be derived:

$$c_{\mathrm{f}}\mathbb{E}^{\mathrm{f}} = \left(\mathbb{L}^{\mathrm{f}} - \mathbb{L}^{\mathrm{m}}\right)^{-1} : \left(\mathbb{L}^{\mathrm{c}} - \mathbb{L}^{\mathrm{m}}\right) \tag{14}$$

In addition, define

$$c_{\mathrm{m}}\mathbb{E}^{\mathrm{m}} \equiv \left(\mathbb{L}^{\mathrm{m}} - \mathbb{L}^{\mathrm{f}}\right)^{-1} : \left(\mathbb{L}^{\mathrm{c}} - \mathbb{L}^{\mathrm{f}}\right) \tag{15}$$

so that

$$c_{\mathrm{a}}\boxed{\mathbb{E}^{\mathrm{a}}} : \mathbb{L}^{\mathrm{m}} : \boxed{\mathbb{E}^{\mathrm{a}}} + c_{\mathrm{b}}\boxed{\mathbb{E}^{\mathrm{b}}} : \mathbb{L}^{\mathrm{m}} : \boxed{\mathbb{E}^{\mathrm{b}}} = \mathbb{L}^{\mathrm{c}} - c_{\mathrm{f}}\mathbb{E}^{\mathrm{f}} : \mathbb{L}^{\mathrm{f}} : \mathbb{E}^{\mathrm{f}} \tag{16}$$

$$c_{\mathrm{a}}\boxed{\mathbb{E}^{\mathrm{a}}} + c_{\mathrm{b}}\boxed{\mathbb{E}^{\mathrm{b}}} = c_{\mathrm{m}}\mathbb{E}^{\mathrm{m}} \tag{17}$$

where boxed tensors are to be determined. Substituting (17) into (16) and eliminating $\left\{\mathbb{E}^{\mathrm{b}}\right\}$ yields

$$\begin{aligned} &c_{\mathrm{a}}c_{\mathrm{b}}\left\{\mathbb{E}^{\mathrm{a}}\right\}^{\mathrm{T}}\left\{\mathbb{L}^{\mathrm{m}}\right\}\left\{\mathbb{E}^{\mathrm{a}}\right\} + \left[c_{\mathrm{a}}\left\{\mathbb{E}^{\mathrm{a}}\right\} - c_{\mathrm{m}}\left\{\mathbb{E}^{\mathrm{m}}\right\}\right]^{\mathrm{T}}\left\{\mathbb{L}^{\mathrm{m}}\right\}\left[c_{\mathrm{a}}\left\{\mathbb{E}^{\mathrm{a}}\right\} - c_{\mathrm{m}}\left\{\mathbb{E}^{\mathrm{m}}\right\}\right] \\ &\quad = c_{\mathrm{b}}\left\{\mathbb{L}^{\mathrm{c}}\right\} - c_{\mathrm{b}}c_{\mathrm{f}}\left\{\mathbb{E}^{\mathrm{f}}\right\}^{\mathrm{T}}\left\{\mathbb{L}^{\mathrm{f}}\right\}\left\{\mathbb{E}^{\mathrm{f}}\right\} \end{aligned} \tag{18}$$

Rearranging (18) yields

$$\left[\left\{\mathbb{E}^{\mathrm{a}}\right\} - \left\{\mathbb{E}^{\mathrm{m}}\right\}\right]^{\mathrm{T}}\left\{\mathbb{L}^{\mathrm{m}}\right\}\left[\left\{\mathbb{E}^{\mathrm{a}}\right\} - \left\{\mathbb{E}^{\mathrm{m}}\right\}\right] = \frac{c_{\mathrm{b}}/c_{\mathrm{a}}}{c_{\mathrm{m}}}\left[\left\{\mathbb{L}^{\mathrm{c}}\right\} - c_{\mathrm{f}}\left\{\mathbb{E}^{\mathrm{f}}\right\}^{\mathrm{T}}\left\{\mathbb{L}^{\mathrm{f}}\right\}\left\{\mathbb{E}^{\mathrm{f}}\right\} - c_{\mathrm{m}}\left\{\mathbb{E}^{\mathrm{m}}\right\}^{\mathrm{T}}\left\{\mathbb{L}^{\mathrm{m}}\right\}\left\{\mathbb{E}^{\mathrm{m}}\right\}\right] \tag{19}$$

Similarly, substituting (17) into (16) and eliminating $\{\mathbb{E}^{\mathrm{a}}\}$ yield

$$\left[\left\{\mathbb{E}^{\mathrm{b}}\right\}-\left\{\mathbb{E}^{\mathrm{m}}\right\}\right]^{\mathrm{T}}\left\{\mathbb{L}^{\mathrm{m}}\right\}\left[\left\{\mathbb{E}^{\mathrm{b}}\right\}-\left\{\mathbb{E}^{\mathrm{m}}\right\}\right]=\frac{c_{\mathrm{a}}/c_{\mathrm{b}}}{c_{\mathrm{m}}}\left[\left\{\mathbb{L}^{\mathrm{c}}\right\}-c_{\mathrm{f}}\left\{\mathbb{E}^{\mathrm{f}}\right\}^{\mathrm{T}}\left\{\mathbb{L}^{\mathrm{f}}\right\}\left\{\mathbb{E}^{\mathrm{f}}\right\}-c_{\mathrm{m}}\left\{\mathbb{E}^{\mathrm{m}}\right\}^{\mathrm{T}}\left\{\mathbb{L}^{\mathrm{m}}\right\}\left\{\mathbb{E}^{\mathrm{m}}\right\}\right] \tag{20}$$

The right-hand-side term in (19) and (20) can be proved as semi-positive-definite. The proof is given in Appendix A. Suppose

$$\{\Delta\mathbb{L}\}=\left\{\mathbb{L}^{\mathrm{c}}\right\}-c_{\mathrm{f}}\left\{\mathbb{E}^{\mathrm{f}}\right\}^{\mathrm{T}}\left\{\mathbb{L}^{\mathrm{f}}\right\}\left\{\mathbb{E}^{\mathrm{f}}\right\}-c_{\mathrm{m}}\left\{\mathbb{E}^{\mathrm{m}}\right\}^{\mathrm{T}}\left\{\mathbb{L}^{\mathrm{m}}\right\}\left\{\mathbb{E}^{\mathrm{m}}\right\}=\{\mathbb{R}\}^{\mathrm{T}}\{\mathbb{R}\} \tag{21}$$

where $\{\mathbb{R}\}$ is obtained through singular value decomposition (SVD). The first row and column of $\{\Delta\mathbb{L}\}$ are all zeros. Defining that

$$\begin{cases}\{\Delta\mathbb{E}^{\mathrm{a}}\}=\{\mathbb{E}^{\mathrm{a}}\}-\{\mathbb{E}^{\mathrm{m}}\}\\ \left\{\Delta\mathbb{E}^{\mathrm{b}}\right\}=\left\{\mathbb{E}^{\mathrm{b}}\right\}-\{\mathbb{E}^{\mathrm{m}}\}\end{cases} \tag{22}$$

For any macroscopic strain $\{\boldsymbol{\varepsilon}^{\mathrm{c}}\}=[\varepsilon_{11}^{\mathrm{c}},0,0,0,0,0]^{\mathrm{T}}$, the following equation can always be fulfilled:

$$\begin{aligned}&\{\boldsymbol{\varepsilon}^{\mathrm{c}}\}^{\mathrm{T}}\{\Delta\mathbb{L}\}\{\boldsymbol{\varepsilon}^{\mathrm{c}}\}\\ &=\frac{c_{\mathrm{m}}c_{\mathrm{a}}}{c_{\mathrm{b}}}\{\boldsymbol{\varepsilon}^{\mathrm{c}}\}^{\mathrm{T}}\{\Delta\mathbb{E}^{\mathrm{a}}\}^{\mathrm{T}}\{\mathbb{L}^{\mathrm{m}}\}\{\Delta\mathbb{E}^{\mathrm{a}}\}\{\boldsymbol{\varepsilon}^{\mathrm{c}}\}\\ &=\frac{c_{\mathrm{m}}c_{\mathrm{b}}}{c_{\mathrm{a}}}\{\boldsymbol{\varepsilon}^{\mathrm{c}}\}^{\mathrm{T}}\left\{\Delta\mathbb{E}^{\mathrm{b}}\right\}^{\mathrm{T}}\{\mathbb{L}^{\mathrm{m}}\}\left\{\Delta\mathbb{E}^{\mathrm{b}}\right\}\{\boldsymbol{\varepsilon}^{\mathrm{c}}\}\\ &=0\end{aligned} \tag{23}$$

Due to the positive definiteness of $\{\mathbb{L}^{\mathrm{m}}\}$, the first columns of $\{\Delta\mathbb{E}^{\mathrm{a}}\}$ and $\left\{\Delta\mathbb{E}^{\mathrm{b}}\right\}$ are all zeros. In addition, the strain along the longitudinal direction within the matrix should be uniform. That yields that the first rows of $\{\mathbb{E}^{\mathrm{m}}\}$, $\{\mathbb{E}^{\mathrm{a}}\}$, and $\left\{\mathbb{E}^{\mathrm{b}}\right\}$ are the same so that the first rows of $\{\Delta\mathbb{E}^{\mathrm{a}}\}$ and $\left\{\Delta\mathbb{E}^{\mathrm{b}}\right\}$ are also zeros. Then $\{\Delta\mathbb{E}^{\mathrm{a}}\}$ and $\left\{\Delta\mathbb{E}^{\mathrm{b}}\right\}$ can be written as follows:

$$\{\Delta\mathbb{E}^{\mathrm{a}}\}=\begin{bmatrix}0 & \mathbf{0}^{\mathrm{T}}\\ \mathbf{0} & \Delta\boldsymbol{E}^{\mathrm{a}}\end{bmatrix}\quad\left\{\Delta\mathbb{E}^{\mathrm{b}}\right\}=\begin{bmatrix}0 & \mathbf{0}^{\mathrm{T}}\\ \mathbf{0} & \Delta\boldsymbol{E}^{\mathrm{b}}\end{bmatrix} \tag{24}$$

where $\Delta\boldsymbol{E}^{\mathrm{a}}$ and $\Delta\boldsymbol{E}^{\mathrm{b}}$ are 5×5 matrices to be solved. Finally, without losing generosity, it obtains the solution for $\{\mathbb{E}^{\mathrm{a}}\}$ and $\left\{\mathbb{E}^{\mathrm{b}}\right\}$ that

$$\begin{cases}\{\mathbb{E}^{\mathrm{a}}\}=\{\mathbb{E}^{\mathrm{m}}\}+\sqrt{\dfrac{c_{\mathrm{b}}/c_{\mathrm{a}}}{c_{\mathrm{a}}+c_{\mathrm{b}}}}\{\mathbb{V}^{\mathrm{m}}\}\{\mathbb{R}\}\\ \left\{\mathbb{E}^{\mathrm{b}}\right\}=\{\mathbb{E}^{\mathrm{m}}\}-\sqrt{\dfrac{c_{\mathrm{a}}/c_{\mathrm{b}}}{c_{\mathrm{a}}+c_{\mathrm{b}}}}\{\mathbb{V}^{\mathrm{m}}\}\{\mathbb{R}\}\end{cases} \tag{25}$$

where $c_{\mathrm{m}}=c_{\mathrm{a}}+c_{\mathrm{b}}$ is substituted and the detailed process of calculation for $\{\mathbb{V}^{\mathrm{m}}\}$ and $\{\mathbb{R}\}$ is given in Appendix B.

3.2 Eigenstrain Influence Functions

For the fibrous unitcell with 1 + 2 partitions, the reduced-order system of equations is derived from (2) that

$$\boldsymbol{\varepsilon}^{\mathtt{f}} - \mathbb{P}^{\mathtt{ff}} : \boldsymbol{\mu}^{\mathtt{f}} - \mathbb{P}^{\mathtt{fa}} : \boldsymbol{\mu}^{\mathtt{a}} - \mathbb{P}^{\mathtt{fb}} : \boldsymbol{\mu}^{\mathtt{b}} = \mathbb{E}^{\mathtt{f}} : \boldsymbol{\varepsilon}^{\mathtt{c}} \tag{26}$$

$$\boldsymbol{\varepsilon}^{\mathtt{a}} - \mathbb{P}^{\mathtt{af}} : \boldsymbol{\mu}^{\mathtt{f}} - \mathbb{P}^{\mathtt{aa}} : \boldsymbol{\mu}^{\mathtt{a}} - \mathbb{P}^{\mathtt{ab}} : \boldsymbol{\mu}^{\mathtt{b}} = \mathbb{E}^{\mathtt{a}} : \boldsymbol{\varepsilon}^{\mathtt{c}} \tag{27}$$

$$\boldsymbol{\varepsilon}^{\mathtt{b}} - \mathbb{P}^{\mathtt{bf}} : \boldsymbol{\mu}^{\mathtt{f}} - \mathbb{P}^{\mathtt{ba}} : \boldsymbol{\mu}^{\mathtt{a}} - \mathbb{P}^{\mathtt{bb}} : \boldsymbol{\mu}^{\mathtt{b}} = \mathbb{E}^{\mathtt{b}} : \boldsymbol{\varepsilon}^{\mathtt{c}} \tag{28}$$

The eigenstrain influence tensors satisfy the following constraints (Chapter 4 of the textbook [52]):

$$\mathbb{P}^{\mathtt{ff}} + \mathbb{P}^{\mathtt{fa}} + \mathbb{P}^{\mathtt{fb}} = \mathbb{I} - \mathbb{E}^{\mathtt{f}} \tag{29}$$

$$\mathbb{P}^{\mathtt{af}} + \mathbb{P}^{\mathtt{aa}} + \mathbb{P}^{\mathtt{ab}} = \mathbb{I} - \mathbb{E}^{\mathtt{a}} \tag{30}$$

$$\mathbb{P}^{\mathtt{bf}} + \mathbb{P}^{\mathtt{ba}} + \mathbb{P}^{\mathtt{bb}} = \mathbb{I} - \mathbb{E}^{\mathtt{b}} \tag{31}$$

This constructs two special cases with perfect plastic yielding at selected partition(s) to solve the eigenstrain influence functions. For Case I, it asks that the outer partition of the matrix gets perfect plastic yielding while the inner partition of the matrix and the fiber phase remain elastic. For Case II, it assumes that the whole matrix phase gets perfect plastic yield while the fiber is still elastic. A sketch of two cases is depicted in Fig. 3.

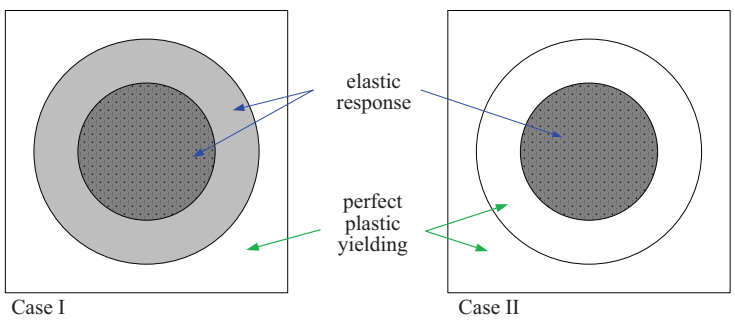

Figure 3: Sketch of two cases with perfect plastic yielding at selected partition(s)

3.2.1 Case I

In the first case, under macroscopic strain $\boldsymbol{\varepsilon}^{\mathtt{c}}$, the strains at the fiber phase and the inner partition of the matrix phase are given as follows:

$$\boldsymbol{\varepsilon}^{\mathtt{f}} = \begin{bmatrix} 1 & -\nu_{\mathrm{I}}^{\mathtt{f}} & -\nu_{\mathrm{I}}^{\mathtt{f}} & 0 & 0 & 0 \end{bmatrix}^{\mathrm{T}} \cdot \varepsilon_{11}^{\mathtt{c}} \equiv \begin{bmatrix} 1 & \boldsymbol{e}_{\mathrm{I}}^{\mathtt{f},\mathrm{I}} \end{bmatrix}^{\mathrm{T}} \cdot \varepsilon_{11}^{\mathtt{c}} \tag{32}$$

$$\boldsymbol{\varepsilon}^{\mathtt{a}} = \begin{bmatrix} 1 & -\nu_{\mathrm{I}}^{\mathtt{a}} & -\nu_{\mathrm{I}}^{\mathtt{a}} & 0 & 0 & 0 \end{bmatrix}^{\mathrm{T}} \cdot \varepsilon_{11}^{\mathtt{c}} \equiv \begin{bmatrix} 1 & \boldsymbol{e}_{\mathrm{I}}^{\mathtt{a},\mathrm{I}} \end{bmatrix}^{\mathrm{T}} \cdot \varepsilon_{11}^{\mathtt{c}} \tag{33}$$

respectively, with

$$\nu_{\mathrm{I}}^{\mathtt{f}} = \nu_{\mathrm{at}}^{\mathtt{f}} + \frac{c_{\mathtt{a}}\varphi(1-2\nu^{\mathtt{m}})(\nu^{\mathtt{m}} - \nu_{\mathrm{at}}^{\mathtt{f}})}{2c_{\mathtt{f}}(1-\nu^{\mathtt{m}}) + c_{\mathtt{a}}(1+\varphi(1-2\nu^{\mathtt{m}}))} \tag{34}$$

$$\nu_{\mathrm{I}}^{\mathtt{a}} = \nu^{\mathtt{m}} - \frac{c_{\mathtt{f}}(1-2\nu^{\mathtt{m}})(\nu^{\mathtt{m}} - \nu_{\mathrm{at}}^{\mathtt{f}})}{2c_{\mathtt{f}}(1-\nu^{\mathtt{m}}) + c_{\mathtt{a}}(1+\varphi(1-2\nu^{\mathtt{m}}))} + \frac{c_{\mathtt{f}}}{c_{\mathtt{a}}} \ln \frac{c_{\mathtt{f}} + c_{\mathtt{a}}}{c_{\mathtt{f}}} \frac{(c_{\mathtt{f}} + c_{\mathtt{a}})(\nu^{\mathtt{m}} - \nu_{\mathrm{at}}^{\mathtt{f}})}{2c_{\mathtt{f}}(1-\nu^{\mathtt{m}}) + c_{\mathtt{a}}(1+\varphi(1-2\nu^{\mathtt{m}}))} \tag{35}$$

The derivation of the vector components can be seen in Appendix C.

Thus, it can define the so-called *perfect plastic influence function* for the fiber phase and the inner partition of the matrix phase that

$$\left\{\tilde{\mathbb{E}}^{\mathtt{f},\mathrm{I}}\right\} = \begin{bmatrix} 1 & \boldsymbol{0}^{\mathrm{T}} \\ \boldsymbol{e}_1^{\mathtt{f},\mathrm{I}} & \boldsymbol{O}_5 \end{bmatrix} \tag{36}$$

and

$$\left\{\tilde{\mathbb{E}}^{\mathtt{a},\mathrm{I}}\right\} = \begin{bmatrix} 1 & \boldsymbol{0}^{\mathrm{T}} \\ \boldsymbol{e}_1^{\mathtt{a},\mathrm{I}} & \boldsymbol{O}_5 \end{bmatrix} \tag{37}$$

respectively, with $\boldsymbol{O}_n$ is a full 0 matrix with size $n \times n$. The "perfect plastic" emphasizes that the strain influence functions are associated with specific material yielding status. The strain influence function for the outer partition of the matrix phase is first written as follows:

$$\left\{\tilde{\mathbb{E}}^{\mathtt{b},\mathrm{I}}\right\} = \begin{bmatrix} 1 & \boldsymbol{0}^{\mathrm{T}} \\ \boldsymbol{e}_1^{\mathtt{b},\mathrm{I}} & \tilde{\boldsymbol{E}}^{\mathtt{b},\mathrm{I}} \end{bmatrix} \tag{38}$$

For the fiber-dominated mode, i.e., the longitudinal direction, $\boldsymbol{e}_1^{\mathtt{b},\mathrm{I}}$ is determined by the constraint condition (3) that

$$\boldsymbol{e}_1^{\mathtt{b},\mathrm{I}} = \frac{1}{c_{\mathtt{b}}}\left[-c_{\mathtt{f}}\boldsymbol{e}_1^{\mathtt{f},\mathrm{I}} - c_{\mathtt{a}}\boldsymbol{e}_1^{\mathtt{a},\mathrm{I}}\right] = \begin{bmatrix} -\nu_{\mathrm{I}}^{\mathtt{b}} & -\nu_{\mathrm{I}}^{\mathtt{b}} & 0 & 0 & 0 \end{bmatrix}^{\mathrm{T}} \tag{39}$$

with

$$\begin{aligned} \nu_{\mathrm{I}}^{\mathtt{b}} = &-\frac{c_{\mathtt{f}}\nu_{\mathrm{at}}^{\mathtt{f}} + c_{\mathtt{a}}\nu^{\mathtt{m}}}{c_{\mathtt{b}}} - \frac{c_{\mathtt{a}}c_{\mathtt{f}}}{c_{\mathtt{b}}}\frac{(\varphi-1)(1-2\nu^{\mathtt{m}})(\nu^{\mathtt{m}}-\nu_{\mathrm{at}}^{\mathtt{f}})}{2c_{\mathtt{f}}(1-\nu^{\mathtt{m}}) + c_{\mathtt{a}}(1+\varphi(1-2\nu^{\mathtt{m}}))} \\ &- \frac{c_{\mathtt{f}}}{c_{\mathtt{b}}}\ln\frac{c_{\mathtt{f}}+c_{\mathtt{a}}}{c_{\mathtt{f}}}\frac{(c_{\mathtt{f}}+c_{\mathtt{a}})(\nu^{\mathtt{m}}-\nu_{\mathrm{at}}^{\mathtt{f}})}{2c_{\mathtt{f}}(1-\nu^{\mathtt{m}}) + c_{\mathtt{a}}(1+\varphi(1-2\nu^{\mathtt{m}}))} \end{aligned} \tag{40}$$

The sub-matrix $\tilde{\boldsymbol{E}}^{\mathtt{b},\mathrm{I}}$ defined in (38) is calculated by the effort of eliminating the so-called "inclusion-locking" phenomenon. With arbitrary macroscopic incremental strain $\Delta\boldsymbol{\varepsilon}^{\mathtt{c}}$ with $\Delta\varepsilon_{11}^{\mathtt{c}} = 0$, it asks for the contribution of the fiber phase and inner partition of the matrix phase to the macroscopic stress is 0, i.e.,

$$\mathbb{L}^{\mathtt{c}} : \Delta\boldsymbol{\varepsilon}^{\mathtt{c}} = c_{\mathtt{b}}\mathbb{L}^{\mathtt{m}} : \Delta\boldsymbol{\varepsilon}^{\mathtt{b}} = c_{\mathtt{b}}\mathbb{L}^{\mathtt{m}} : \tilde{\mathbb{E}}^{\mathtt{b},\mathrm{I}} : \Delta\boldsymbol{\varepsilon}^{\mathtt{c}} \tag{41}$$

with the arbitrariness of $\Delta\boldsymbol{\varepsilon}^{\mathtt{c}}$ with $\Delta\varepsilon_{11}^{\mathtt{c}} = 0$, it can obtain $\tilde{\boldsymbol{E}}^{\mathtt{b},\mathrm{I}}$ through (41) satisfying

$$\left\{\begin{bmatrix} 1 & (\boldsymbol{l}_1^{\mathtt{c}})^{\mathrm{T}} \\ \boldsymbol{l}_1^{\mathtt{c}} & \boldsymbol{L}^{\mathtt{c}} \end{bmatrix} - c_{\mathtt{b}}\begin{bmatrix} 1 & (\boldsymbol{l}_1^{\mathtt{m}})^{\mathrm{T}} \\ \boldsymbol{l}_1^{\mathtt{m}} & \boldsymbol{L}^{\mathtt{m}} \end{bmatrix}\begin{bmatrix} 1 & \boldsymbol{0}^{\mathrm{T}} \\ \boldsymbol{e}_1^{\mathtt{b},\mathrm{I}} & \tilde{\boldsymbol{E}}^{\mathtt{b},\mathrm{I}} \end{bmatrix}\right\}\begin{bmatrix} 0 \\ \Delta\varepsilon_{22} \\ \Delta\varepsilon_{33} \\ \Delta\varepsilon_{23} \\ \Delta\varepsilon_{13} \\ \Delta\varepsilon_{12} \end{bmatrix} = \begin{bmatrix} 0 \\ 0 \\ 0 \\ 0 \\ 0 \\ 0 \end{bmatrix}, \quad \forall\Delta\varepsilon_{ij}, ij = 22, 33, 23, 13, 12 \tag{42}$$

Once the perfect plastic influence functions for all partitions are determined, the eigenstrain influence functions $\mathbb{P}^{\mathtt{bb}}$, $\mathbb{P}^{\mathtt{ba}}$, and $\mathbb{P}^{\mathtt{bf}}$ can be computed one after another. The reduced-order model is supposed given by an incremental macroscopic strain $\Delta\boldsymbol{\varepsilon}^{\mathtt{c}}$. By the assumption that the fiber and the inner partition of the

matrix phase remain elastic while the outer partition of the matrix phase gets yield, it has $\Delta\boldsymbol{\mu}^{\mathrm{f}} = \Delta\boldsymbol{\mu}^{\mathrm{a}} = \mathbf{0}$, and $\Delta\boldsymbol{\varepsilon}^{\mathrm{b}} = \Delta\boldsymbol{\mu}^{\mathrm{b}}$. Accordingly, (26)–(28) are rewritten as follows:

$$\Delta\boldsymbol{\varepsilon}^{\mathrm{f}} - \mathbb{P}^{\mathrm{fb}} : \Delta\boldsymbol{\varepsilon}^{\mathrm{b}} = \mathbb{E}^{\mathrm{f}} : \Delta\boldsymbol{\varepsilon}^{\mathrm{c}} \tag{43}$$

$$\Delta\boldsymbol{\varepsilon}^{\mathrm{a}} - \mathbb{P}^{\mathrm{ab}} : \Delta\boldsymbol{\varepsilon}^{\mathrm{b}} = \mathbb{E}^{\mathrm{a}} : \Delta\boldsymbol{\varepsilon}^{\mathrm{c}} \tag{44}$$

$$\Delta\boldsymbol{\varepsilon}^{\mathrm{b}} - \mathbb{P}^{\mathrm{bb}} : \Delta\boldsymbol{\varepsilon}^{\mathrm{b}} = \mathbb{E}^{\mathrm{b}} : \Delta\boldsymbol{\varepsilon}^{\mathrm{c}} \tag{45}$$

From (45), it can find

$$\Delta\boldsymbol{\varepsilon}^{\mathrm{b}} = (\mathbb{I} - \mathbb{P}^{\mathrm{bb}})^{-1} : \mathbb{E}^{\mathrm{b}} : \Delta\boldsymbol{\varepsilon}^{\mathrm{c}} = \tilde{\mathbb{E}}^{\mathrm{b,I}} : \Delta\boldsymbol{\varepsilon}^{\mathrm{c}} \Rightarrow \mathbb{P}^{\mathrm{bb}} = \mathbb{I} - \mathbb{E}^{\mathrm{b}} : (\tilde{\mathbb{E}}^{\mathrm{b,I}})^{-1} \tag{46}$$

Through (43) and (44), it can obtain

$$\Delta\boldsymbol{\varepsilon}^{\mathrm{f}} = (\mathbb{P}^{\mathrm{fb}} : \tilde{\mathbb{E}}^{\mathrm{b,I}} + \mathbb{E}^{\mathrm{f}}) : \Delta\boldsymbol{\varepsilon}^{\mathrm{c}} = \tilde{\mathbb{E}}^{\mathrm{f,I}} : \Delta\boldsymbol{\varepsilon}^{\mathrm{c}} \Rightarrow \mathbb{P}^{\mathrm{fb}} = (\tilde{\mathbb{E}}^{\mathrm{f,I}} - \mathbb{E}^{\mathrm{f}}) : (\tilde{\mathbb{E}}^{\mathrm{b,I}})^{-1} \tag{47}$$

and

$$\Delta\boldsymbol{\varepsilon}^{\mathrm{a}} = (\mathbb{P}^{\mathrm{ab}} : \tilde{\mathbb{E}}^{\mathrm{b,I}} + \mathbb{E}^{\mathrm{a}}) : \Delta\boldsymbol{\varepsilon}^{\mathrm{c}} = \tilde{\mathbb{E}}^{\mathrm{a,I}} : \Delta\boldsymbol{\varepsilon}^{\mathrm{c}} \Rightarrow \mathbb{P}^{\mathrm{ab}} = (\tilde{\mathbb{E}}^{\mathrm{a,I}} - \mathbb{E}^{\mathrm{a}}) : (\tilde{\mathbb{E}}^{\mathrm{b,I}})^{-1} \tag{48}$$

respectively.

3.2.2 Case II

Case II is studied, where the whole matrix phase gets perfect plastic yield while the fiber is still elastic. Similarly, under macroscopic strain $\boldsymbol{\varepsilon}^{\mathrm{c}}$, the strains at the fiber phase and the inner partition of the matrix phase are given as follows:

$$\boldsymbol{\varepsilon}^{\mathrm{f}} = \begin{bmatrix} 1 & -\nu_{\mathrm{II}}^{\mathrm{f}} & -\nu_{\mathrm{II}}^{\mathrm{f}} & 0 & 0 & 0 \end{bmatrix}^{\mathrm{T}} \cdot \varepsilon_{11}^{\mathrm{c}} \equiv \begin{bmatrix} 1 & \boldsymbol{e}_1^{\mathrm{f,II}} \end{bmatrix}^{\mathrm{T}} \cdot \varepsilon_{11}^{\mathrm{c}} \tag{49}$$

$$\boldsymbol{\varepsilon}^{\mathrm{a}} = \begin{bmatrix} 1 & -\nu_{\mathrm{II}}^{\mathrm{a}} & -\nu_{\mathrm{II}}^{\mathrm{a}} & 0 & 0 & 0 \end{bmatrix}^{\mathrm{T}} \cdot \varepsilon_{11}^{\mathrm{c}} \equiv \begin{bmatrix} 1 & \boldsymbol{e}_1^{\mathrm{a,II}} \end{bmatrix}^{\mathrm{T}} \cdot \varepsilon_{11}^{\mathrm{c}} \tag{50}$$

respectively. The effective Poisson's ratio $\nu_{\mathrm{II}}^{\mathrm{f}}$ and $\nu_{\mathrm{II}}^{\mathrm{a}}$ can be derived similarly but $\varphi = 0$ as (34) and (35), respectively, that

$$\nu_{\mathrm{II}}^{\mathrm{f}} = \nu_{\mathrm{at}}^{\mathrm{f}} \tag{51}$$

$$\nu_{\mathrm{II}}^{\mathrm{a}} = \nu^{\mathrm{m}} - \frac{c_{\mathrm{f}}(1 - 2\nu^{\mathrm{m}})(\nu^{\mathrm{m}} - \nu_{\mathrm{at}}^{\mathrm{f}})}{2c_{\mathrm{f}}(1 - \nu^{\mathrm{m}}) + c_{\mathrm{a}}} + \frac{c_{\mathrm{f}}}{c_{\mathrm{a}}} \ln \frac{c_{\mathrm{f}} + c_{\mathrm{a}}}{c_{\mathrm{f}}} \frac{(c_{\mathrm{f}} + c_{\mathrm{a}})(\nu^{\mathrm{m}} - \nu_{\mathrm{at}}^{\mathrm{f}})}{2c_{\mathrm{f}}(1 - \nu^{\mathrm{m}}) + c_{\mathrm{a}}} \tag{52}$$

Thus, it can define the perfect plastic influence function for the fiber phase and the inner partition of the matrix phase that

$$\left\{\tilde{\mathbb{E}}^{\mathrm{f,II}}\right\} = \begin{bmatrix} 1 & \mathbf{0}^{\mathrm{T}} \\ \boldsymbol{e}_1^{\mathrm{f,II}} & \boldsymbol{O}_5 \end{bmatrix} \tag{53}$$

and

$$\left\{\tilde{\mathbb{E}}^{\mathrm{a,II}}\right\} = \begin{bmatrix} 1 & \mathbf{0}^{\mathrm{T}} \\ \boldsymbol{e}_1^{\mathrm{a,II}} & \boldsymbol{O}_5 \end{bmatrix} \tag{54}$$

The strain influence function for the outer partition of the matrix phase is first written as follows:

$$\left\{\tilde{\mathbb{E}}^{\mathrm{b,II}}\right\} = \begin{bmatrix} 1 & \mathbf{0}^{\mathrm{T}} \\ \boldsymbol{e}_1^{\mathrm{b,II}} & \tilde{\boldsymbol{E}}^{\mathrm{b,II}} \end{bmatrix} \tag{55}$$

For the fiber-dominated mode, i.e., the longitudinal direction, $\boldsymbol{e}_1^{\mathrm{b,II}}$ is determined by the constraint condition (3) that

$$\boldsymbol{e}_1^{\mathrm{b,II}} = \frac{1}{c_{\mathrm{b}}}\left(-c_{\mathrm{f}}\boldsymbol{e}_1^{\mathrm{f,II}} - c_{\mathrm{a}}\boldsymbol{e}_1^{\mathrm{a,II}}\right) = \begin{bmatrix} -\nu_{\mathrm{II}}^{\mathrm{b}} & -\nu_{\mathrm{II}}^{\mathrm{b}} & 0 & 0 & 0 \end{bmatrix}^{\mathrm{T}} \tag{56}$$

with

$$\nu_{\mathrm{II}}^{\mathrm{b}} = -\frac{c_{\mathrm{f}}\nu_{\mathrm{at}}^{\mathrm{f}} + c_{\mathrm{a}}\nu^{\mathrm{m}}}{c_{\mathrm{b}}} + \frac{c_{\mathrm{a}}c_{\mathrm{f}}}{c_{\mathrm{b}}}\frac{(1-2\nu^{\mathrm{m}})(\nu^{\mathrm{m}}-\nu_{\mathrm{at}}^{\mathrm{f}})}{2c_{\mathrm{f}}(1-\nu^{\mathrm{m}})+c_{\mathrm{a}}} - \frac{c_{\mathrm{f}}}{c_{\mathrm{b}}}\ln\frac{c_{\mathrm{f}}+c_{\mathrm{a}}}{c_{\mathrm{f}}}\frac{(c_{\mathrm{f}}+c_{\mathrm{a}})(\nu^{\mathrm{m}}-\nu_{\mathrm{at}}^{\mathrm{f}})}{2c_{\mathrm{f}}(1-\nu^{\mathrm{m}})+c_{\mathrm{a}}} \tag{57}$$

The sub-matrix $\tilde{\boldsymbol{E}}^{\mathrm{b,II}}$ defined in (38) is calculated by the effort of eliminating the so-called "inclusion-locking" phenomenon. With arbitrary macroscopic incremental strain $\Delta\boldsymbol{\varepsilon}^{\mathrm{c}}$ with $\Delta\varepsilon_{11}^{\mathrm{c}} = 0$, it asks for the contribution of the fiber phase and inner partition of the matrix phase to the macroscopic stress is 0, i.e.,

$$\mathbb{L}^{\mathrm{c}} : \Delta\boldsymbol{\varepsilon}^{\mathrm{c}} = c_{\mathrm{b}}\mathbb{L}^{\mathrm{m}} : \Delta\boldsymbol{\varepsilon}^{\mathrm{b}} = c_{\mathrm{b}}\mathbb{L}^{\mathrm{m}} : \tilde{\mathbb{E}}^{\mathrm{b,II}} : \Delta\boldsymbol{\varepsilon}^{\mathrm{c}} \tag{58}$$

with the arbitrariness of $\Delta\boldsymbol{\varepsilon}^{\mathrm{c}}$ with $\Delta\varepsilon_{11}^{\mathrm{c}} = 0$, it can obtain $\tilde{\boldsymbol{E}}^{\mathrm{b,II}}$ through (58).

3.3 Volume Fraction of Inner and Outer Matrix Partitions

The purpose of searching for the optimum volume fraction of inner matrix partition c_{a} is to minimize the average error of strain energy density within the matrix phase domain between 1 + 2 partition ROH model and Eshelby tensor solution in a given unit macroscopic strain loading space, written as $\mathcal{L}$. The average of squared error of strain energy density within matrix domain $\overline{\mathcal{D}}_{\mathrm{u}}$ under given c_{a} and macroscopic strain loading $\boldsymbol{\varepsilon}^{\mathrm{c}}$ is expressed as follows:

$$\overline{\mathcal{D}}_{\mathrm{u}}(c_{\mathrm{a}}, \boldsymbol{\varepsilon}^{\mathrm{c}}) = \frac{1}{\Theta^{\mathrm{m}}}\left[\int_{\Theta^{\mathrm{a}}}(\mathcal{U}^{\mathrm{m}}(\mathbf{x}, \boldsymbol{\varepsilon}^{\mathrm{c}}) - \overline{\mathcal{U}}^{\mathrm{a}}(c_{\mathrm{a}}, \boldsymbol{\varepsilon}^{\mathrm{c}}))^2 d\Theta + \int_{\Theta^{\mathrm{b}}}(\mathcal{U}^{\mathrm{m}}(\mathbf{x}, \boldsymbol{\varepsilon}^{\mathrm{c}}) - \overline{\mathcal{U}}^{\mathrm{b}}(c_{\mathrm{a}}, \boldsymbol{\varepsilon}^{\mathrm{c}}))^2 d\Theta\right] \tag{59}$$

where

$$\mathcal{U}^{\mathrm{m}}(\mathbf{x}, \boldsymbol{\varepsilon}^{\mathrm{c}}) = \frac{1}{2}\boldsymbol{\varepsilon}^{\mathrm{m}}(\mathbf{x}, \boldsymbol{\varepsilon}^{\mathrm{c}}) : \mathbb{L}^{\mathrm{m}} : \boldsymbol{\varepsilon}^{\mathrm{m}}(\mathbf{x}, \boldsymbol{\varepsilon}^{\mathrm{c}}), \quad \mathbf{x} \in \Theta^{\mathrm{m}} \tag{60}$$

$$\overline{\mathcal{U}}^{\mathrm{a}}(c_{\mathrm{a}}, \boldsymbol{\varepsilon}^{\mathrm{c}}) = \frac{1}{2}\boldsymbol{\varepsilon}^{\mathrm{c}} : \mathbb{E}^{\mathrm{a}}(c_{\mathrm{a}}) : \mathbb{L}^{\mathrm{m}} : \mathbb{E}^{\mathrm{a}}(c_{\mathrm{a}}) : \boldsymbol{\varepsilon}^{\mathrm{c}} \tag{61}$$

$$\overline{\mathcal{U}}^{\mathrm{b}}(c_{\mathrm{a}}, \boldsymbol{\varepsilon}^{\mathrm{c}}) = \frac{1}{2}\boldsymbol{\varepsilon}^{\mathrm{c}} : \mathbb{E}^{\mathrm{b}}(c_{\mathrm{a}}) : \mathbb{L}^{\mathrm{m}} : \mathbb{E}^{\mathrm{b}}(c_{\mathrm{a}}) : \boldsymbol{\varepsilon}^{\mathrm{c}} \tag{62}$$

$\mathcal{U}^{\mathrm{m}}(\mathbf{x}, \boldsymbol{\varepsilon}^{\mathrm{c}})$ is the strain energy density distribution within the matrix domain. $\overline{\mathcal{U}}^{\mathrm{a}}$ and $\overline{\mathcal{U}}^{\mathrm{b}}$ are the average strain energy densities of inner and outer matrix partitions, respectively, obtained through the 1 + 2 partition ROH model. The strain distribution within the matrix phase domain $\boldsymbol{\varepsilon}^{\mathrm{m}}(\mathbf{x})$ is calculated by an Eshelby tensor method for finite-domain problems [48]:

$$\boldsymbol{\varepsilon}^{\mathrm{m}}(\mathbf{x}) = \boldsymbol{\varepsilon}^{\mathrm{m}} + \boldsymbol{\varepsilon}^{\mathrm{mD}}(\mathbf{x}) = \boldsymbol{\varepsilon}^{\mathrm{m}} + (\mathbb{S}^{\mathrm{m}}(\mathbf{x}) + \mathbb{S}^{\mathrm{BF}}(\mathbf{x})) : \boldsymbol{\varepsilon}^{*}, \quad \mathbf{x} \in \Theta^{\mathrm{m}} \tag{63}$$

$\mathbb{S}^{\mathrm{f}}$ and $\mathbb{S}^{\mathrm{m}}(\mathbf{x})$ ($\mathbf{x} \in \Theta^{\mathrm{m}}$) are classical Eshelby tensors of the fiber domain and matrix domain, respectively, for cylindrical inclusion problem based on infinite matrix assumption, and $\mathbb{S}^{\mathrm{BF}}(\mathbf{x})$ is the modified tensor for the finite matrix domain condition. Their non-zero components are given in Appendix D. $\boldsymbol{\varepsilon}^{\mathrm{mD}}(\mathbf{x})$ is the strain disturbance within the matrix phase. $\boldsymbol{\varepsilon}^{*}$ is the uniform equivalent eigenstrain within the fiber domain induced by inhomogeneity. The study assumes that component $\varepsilon_{11}^{*} = 0$. As the uniform strain field within the fiber domain can be obtained directly by the elastic strain influence functions, the strain disturbance within fiber $\boldsymbol{\varepsilon}^{\mathrm{fD}}$ and $\boldsymbol{\varepsilon}^{*}$ can be calculated by the following equation:

$$\left(\mathbb{S}^{\mathrm{f}} + \left\langle \mathbb{S}^{\mathrm{BF}}(\mathbf{x}) \right\rangle_{\Theta^{\mathrm{f}}}\right) : \boldsymbol{\varepsilon}^{*} = \boldsymbol{\varepsilon}^{\mathrm{fD}} = \boldsymbol{\varepsilon}^{\mathrm{f}} - \boldsymbol{\varepsilon}^{\mathrm{m}} = \left[\mathbb{E}^{\mathrm{f}} : \left(\mathbb{E}^{\mathrm{m}}\right)^{-1} - \mathbb{I}\right] : \boldsymbol{\varepsilon}^{\mathrm{m}} \tag{64}$$

Then (64) yields $\boldsymbol{\varepsilon}^{*} = \mathbb{A} : \boldsymbol{\varepsilon}^{\mathrm{m}}$.

The average $\overline{\mathcal{D}}_{\mathrm{u}}(c_{\mathrm{a}}, \boldsymbol{\varepsilon}^{\mathrm{c}})$ within loading space $\mathcal{L}$ is written as follows:

$$\overline{\mathscr{D}}_{\mathrm{u}}(c_{\mathrm{a}}) = \frac{1}{\Omega_{\mathcal{L}}} \int_{\Omega_{\mathcal{L}}} \overline{\mathcal{D}}_{\mathrm{u}}(c_{\mathrm{a}}, \boldsymbol{\varepsilon}^{\mathrm{c}})|_{\boldsymbol{\varepsilon}^{\mathrm{c}} \in \Omega_{\mathcal{L}}} d\Omega \tag{65}$$

Therefore, the optimum inner matrix partition volume fraction can be calculated by solving the following equation numerically to obtain the extreme point of $\overline{\mathscr{D}}_{\mathrm{u}}(c_{\mathrm{a}})$:

$$\frac{\partial \overline{\mathscr{D}}_{\mathrm{u}}(c_{\mathrm{a}})}{\partial c_{\mathrm{a}}} = 0 \tag{66}$$

This study investigates the nonlinear behaviors of the fibrous composite due to transverse loadings and chooses the following macroscopic strain loading space to search the optimum c_{a}:

$$\mathcal{L} = \left\{\boldsymbol{\varepsilon}^{\mathrm{c}} | \boldsymbol{\varepsilon}^{\mathrm{c}}(\lambda) = \{\mathbb{L}^{\mathrm{c}}\}^{-1}\left[\sqrt{\lambda}\boldsymbol{\sigma}_t^0 + \sqrt{1-\lambda}\boldsymbol{\sigma}_s^0\right], \lambda \in [0,1]\right\} \tag{67}$$

where

$$\boldsymbol{\sigma}_t^0 = \left\{0, 0, \sqrt{\frac{2\mathcal{U}_0}{\{\mathbb{M}^{\mathrm{c}}\}_{33}}}, 0, 0, 0\right\}^{\mathrm{T}} \tag{68}$$

$$\boldsymbol{\sigma}_s^0 = \left\{0, 0, 0, \sqrt{\frac{2\mathcal{U}_0}{\{\mathbb{M}^{\mathrm{c}}\}_{44}}}, 0, 0\right\}^{\mathrm{T}} \tag{69}$$

and $\mathcal{U}_0$ is unit strain energy density, so the corresponding macroscopic strain energy densities of any loadings in $\mathcal{L}$ are the same.

The average strain energy densities of inner and outer matrix partitions under a given global strain loading $\boldsymbol{\varepsilon}^{\mathrm{c}}$ can be written as follows:

$$\begin{aligned}\overline{\mathcal{U}}^{\mathrm{a}} &= \frac{1}{2}\{\boldsymbol{\varepsilon}^{\mathrm{c}}\}^{\mathrm{T}}\{\mathbb{E}^{\mathrm{a}}\}^{\mathrm{T}}\{\mathbb{L}^{\mathrm{m}}\}\{\mathbb{E}^{\mathrm{a}}\}^{\mathrm{T}}\{\boldsymbol{\varepsilon}^{\mathrm{c}}\} \\ &= \frac{1}{2}\{\boldsymbol{\varepsilon}^{\mathrm{c}}\}^{\mathrm{T}}\left[\{\mathbb{E}^{\mathrm{m}}\}^{\mathrm{T}}\{\mathbb{L}^{\mathrm{m}}\}\{\mathbb{E}^{\mathrm{m}}\}^{\mathrm{T}} + \sqrt{\frac{c_{\mathrm{b}}}{c_{\mathrm{a}}}}\frac{1}{\sqrt{c_{\mathrm{m}}}}\left(\{\mathbb{R}\}^{\mathrm{T}}\{\mathbb{V}^{\mathrm{m}}\}^{\mathrm{T}}\{\mathbb{L}^{\mathrm{m}}\}\{\mathbb{E}^{\mathrm{m}}\} + \{\mathbb{E}^{\mathrm{m}}\}^{\mathrm{T}}\{\mathbb{L}^{\mathrm{m}}\}\{\mathbb{V}^{\mathrm{m}}\}\{\mathbb{R}\}\right)\right. \\ &\quad \left. + \frac{c_{\mathrm{b}}}{c_{\mathrm{a}}}\frac{1}{c_{\mathrm{m}}}\{\mathbb{R}\}^{\mathrm{T}}\{\mathbb{V}^{\mathrm{m}}\}^{\mathrm{T}}\{\mathbb{L}^{\mathrm{m}}\}\{\mathbb{V}^{\mathrm{m}}\}\{\mathbb{R}\}\right]\{\boldsymbol{\varepsilon}^{\mathrm{c}}\}\end{aligned} \tag{70}$$

$$\begin{aligned}\overline{\mathcal{U}}^{\mathrm{b}} &= \frac{1}{2}\{\boldsymbol{\varepsilon}^{\mathrm{c}}\}^{\mathrm{T}}\{\mathbb{E}^{\mathrm{a}}\}^{\mathrm{T}}\{\mathbb{L}^{\mathrm{m}}\}\{\mathbb{E}^{\mathrm{a}}\}^{\mathrm{T}}\{\boldsymbol{\varepsilon}^{\mathrm{c}}\} \\ &= \frac{1}{2}\{\boldsymbol{\varepsilon}^{\mathrm{c}}\}^{\mathrm{T}}\Bigg[\{\mathbb{E}^{\mathrm{m}}\}^{\mathrm{T}}\{\mathbb{L}^{\mathrm{m}}\}\{\mathbb{E}^{\mathrm{m}}\}^{\mathrm{T}} - \sqrt{\frac{c_{\mathrm{a}}}{c_{\mathrm{b}}}}\frac{1}{\sqrt{c_{\mathrm{m}}}}\Big(\{\mathbb{R}\}^{\mathrm{T}}\{\mathbb{V}^{\mathrm{m}}\}^{\mathrm{T}}\{\mathbb{L}^{\mathrm{m}}\}\{\mathbb{E}^{\mathrm{m}}\} + \{\mathbb{E}^{\mathrm{m}}\}^{\mathrm{T}}\{\mathbb{L}^{\mathrm{m}}\}\{\mathbb{V}^{\mathrm{m}}\}\{\mathbb{R}\}\Big) \\ &\quad + \frac{c_{\mathrm{a}}}{c_{\mathrm{b}}}\frac{1}{c_{\mathrm{m}}}\{\mathbb{R}\}^{\mathrm{T}}\{\mathbb{V}^{\mathrm{m}}\}^{\mathrm{T}}\{\mathbb{L}^{\mathrm{m}}\}\{\mathbb{V}^{\mathrm{m}}\}\{\mathbb{R}\}\Bigg]\{\boldsymbol{\varepsilon}^{\mathrm{c}}\}\end{aligned} \tag{71}$$

Since the integrals of $\mathbb{S}^{\mathrm{m}}(\mathbf{x})$ within domains of Θ^{a} and Θ^{b} vanish to zero-tensor, substituting (63), (70), and (71) into (59) yields

$$\begin{aligned}&\overline{\mathcal{D}}_{\mathrm{u}}(c_{\mathrm{a}}, \boldsymbol{\varepsilon}^{\mathrm{c}}(\lambda)) \\ &= \frac{1}{\Theta^{\mathrm{m}}}\Bigg[\int_{\Theta}(\mathcal{U}^{\mathrm{m}}(\mathbf{x}, \boldsymbol{\varepsilon}^{\mathrm{c}}))^2 d\Theta + \Theta^{\mathrm{a}}(\overline{\mathcal{U}}^{\mathrm{a}})^2 + \Theta^{\mathrm{b}}(\overline{\mathcal{U}}^{\mathrm{b}})^2 \\ &\quad - \overline{\mathcal{U}}^{\mathrm{a}}\{\boldsymbol{\varepsilon}^{\mathrm{c}}\}^{\mathrm{T}}\{\mathbb{E}^{\mathrm{m}}\}^{\mathrm{T}}\Bigg(\Theta^{\mathrm{a}}\{\mathbb{L}^{\mathrm{m}}\} + \{\mathbb{A}\}^{\mathrm{T}}\int_{\Theta^{\mathrm{a}}}\left\{\mathbb{S}^{\mathrm{BF}}(\mathbf{x})\right\}^{\mathrm{T}} d\Theta\{\mathbb{L}^{\mathrm{m}}\} \\ &\quad + \{\mathbb{L}^{\mathrm{m}}\}\int_{\Theta^{\mathrm{a}}}\left\{\mathbb{S}^{\mathrm{BF}}(\mathbf{x})\right\} d\Theta\{\mathbb{A}\} + \{\mathbb{A}\}^{\mathrm{T}}\int_{\Theta^{\mathrm{a}}}\{\mathbb{B}(\mathbf{x})\} d\Theta\{\mathbb{A}\}\Bigg)\{\mathbb{E}^{\mathrm{m}}\}\{\boldsymbol{\varepsilon}^{\mathrm{c}}\} \\ &\quad - \overline{\mathcal{U}}^{\mathrm{b}}\{\boldsymbol{\varepsilon}^{\mathrm{c}}\}^{\mathrm{T}}\{\mathbb{E}^{\mathrm{m}}\}^{\mathrm{T}}\Bigg(\Theta^{\mathrm{b}}\{\mathbb{L}^{\mathrm{m}}\} + \{\mathbb{A}\}^{\mathrm{T}}\int_{\Theta^{\mathrm{b}}}\left\{\mathbb{S}^{\mathrm{BF}}(\mathbf{x})\right\}^{\mathrm{T}} d\Theta\{\mathbb{L}^{\mathrm{m}}\} \\ &\quad + \{\mathbb{L}^{\mathrm{m}}\}\int_{\Theta^{\mathrm{b}}}\left\{\mathbb{S}^{\mathrm{BF}}(\mathbf{x})\right\} d\Theta\{\mathbb{A}\} + \{\mathbb{A}\}^{\mathrm{T}}\int_{\Theta^{\mathrm{b}}}\{\mathbb{B}(\mathbf{x})\} d\Theta\{\mathbb{A}\}\Bigg)\{\mathbb{E}^{\mathrm{m}}\}\{\boldsymbol{\varepsilon}^{\mathrm{c}}\}\Bigg]\end{aligned} \tag{72}$$

where

$$\begin{aligned}\{\mathbb{B}(\mathbf{x})\} &= \{\mathbb{S}^{\mathrm{m}}(\mathbf{x})\}^{\mathrm{T}}\{\mathbb{L}^{\mathrm{m}}\}\{\mathbb{S}^{\mathrm{m}}(\mathbf{x})\} + \{\mathbb{S}^{\mathrm{m}}(\mathbf{x})\}^{\mathrm{T}}\{\mathbb{L}^{\mathrm{m}}\}\left\{\mathbb{S}^{\mathrm{BF}}(\mathbf{x})\right\} \\ &\quad + \left\{\mathbb{S}^{\mathrm{BF}}(\mathbf{x})\right\}^{\mathrm{T}}\{\mathbb{L}^{\mathrm{m}}\}\{\mathbb{S}^{\mathrm{m}}(\mathbf{x})\} + \left\{\mathbb{S}^{\mathrm{BF}}(\mathbf{x})\right\}^{\mathrm{T}}\{\mathbb{L}^{\mathrm{m}}\}\left\{\mathbb{S}^{\mathrm{BF}}(\mathbf{x})\right\}\end{aligned} \tag{73}$$

Then (66) can be written as follows:

$$\frac{\partial\overline{\mathscr{D}}_{\mathrm{u}}(c_{\mathrm{a}})}{\partial c_{\mathrm{a}}} = \frac{\partial\int_0^1\overline{\mathcal{D}}_{\mathrm{u}}(c_{\mathrm{a}}, \boldsymbol{\varepsilon}^{\mathrm{c}}(\lambda))d\lambda}{\partial c_{\mathrm{a}}} = \int_0^1\frac{\partial\overline{\mathcal{D}}_{\mathrm{u}}(c_{\mathrm{a}}, \boldsymbol{\varepsilon}^{\mathrm{c}}(\lambda))}{\partial c_{\mathrm{a}}}d\lambda \tag{74}$$

while

$$\begin{aligned}&\frac{\partial\overline{\mathcal{D}}_{\mathrm{u}}(c_{\mathrm{a}}, \boldsymbol{\varepsilon}^{\mathrm{c}}(\lambda))}{\partial c_{\mathrm{a}}} \\ &= \frac{1}{\Theta^{\mathrm{m}}}\Bigg[\frac{\Theta^{\mathrm{m}}}{c_{\mathrm{m}}}(\overline{\mathcal{U}}^{\mathrm{a}})^2 - \frac{\Theta^{\mathrm{m}}}{c_{\mathrm{m}}}(\overline{\mathcal{U}}^{\mathrm{b}})^2 + 2\Theta^{\mathrm{a}}\overline{\mathcal{U}}^{\mathrm{a}}\frac{\partial\overline{\mathcal{U}}^{\mathrm{a}}}{\partial c_{\mathrm{a}}} + 2\Theta^{\mathrm{b}}\overline{\mathcal{U}}^{\mathrm{b}}\frac{\partial\overline{\mathcal{U}}^{\mathrm{b}}}{\partial c_{\mathrm{a}}} \\ &\quad - \{\boldsymbol{\varepsilon}^{\mathrm{c}}\}^{\mathrm{T}}\{\mathbb{E}^{\mathrm{m}}\}^{\mathrm{T}}\{\mathbb{L}^{\mathrm{m}}\}\{\mathbb{E}^{\mathrm{m}}\}\{\boldsymbol{\varepsilon}^{\mathrm{c}}\}\left(\frac{\Theta^{\mathrm{m}}}{c_{\mathrm{m}}}\overline{\mathcal{U}}^{\mathrm{a}} - \frac{\Theta^{\mathrm{m}}}{c_{\mathrm{m}}}\overline{\mathcal{U}}^{\mathrm{b}} + \Theta^{\mathrm{a}}\frac{\partial\overline{\mathcal{U}}^{\mathrm{a}}}{\partial c_{\mathrm{a}}} + \Theta^{\mathrm{b}}\frac{\partial\overline{\mathcal{U}}^{\mathrm{b}}}{\partial c_{\mathrm{a}}}\right) \\ &\quad - \frac{\partial\overline{\mathcal{U}}^{\mathrm{a}}}{\partial c_{\mathrm{a}}}\{\boldsymbol{\varepsilon}^{\mathrm{c}}\}^{\mathrm{T}}\{\mathbb{E}^{\mathrm{m}}\}^{\mathrm{T}}\Bigg(\{\mathbb{A}\}^{\mathrm{T}}\int_{\Theta^{\mathrm{a}}}\left\{\mathbb{S}^{\mathrm{BF}}(\mathbf{x})\right\}^{\mathrm{T}} d\Theta\{\mathbb{L}^{\mathrm{m}}\} + \{\mathbb{L}^{\mathrm{m}}\}\int_{\Theta^{\mathrm{a}}}\left\{\mathbb{S}^{\mathrm{BF}}(\mathbf{x})\right\} d\Theta\{\mathbb{A}\} \\ &\quad + \{\mathbb{A}\}^{\mathrm{T}}\int_{\Theta^{\mathrm{a}}}\{\mathbb{B}(\mathbf{x})\} d\Theta\{\mathbb{A}\}\Bigg)\{\mathbb{E}^{\mathrm{m}}\}\{\boldsymbol{\varepsilon}^{\mathrm{c}}\} \\ &\quad - \overline{\mathcal{U}}^{\mathrm{a}}\{\boldsymbol{\varepsilon}^{\mathrm{c}}\}^{\mathrm{T}}\{\mathbb{E}^{\mathrm{m}}\}^{\mathrm{T}}\Bigg(\{\mathbb{A}\}^{\mathrm{T}}\frac{\partial\int_{\Theta^{\mathrm{a}}}\left\{\mathbb{S}^{\mathrm{BF}}(\mathbf{x})\right\}^{\mathrm{T}} d\Theta}{\partial c_{\mathrm{a}}}\{\mathbb{L}^{\mathrm{m}}\} + \{\mathbb{L}^{\mathrm{m}}\}\frac{\partial\int_{\Theta^{\mathrm{a}}}\left\{\mathbb{S}^{\mathrm{BF}}(\mathbf{x})\right\} d\Theta}{\partial c_{\mathrm{a}}}\{\mathbb{A}\}\end{aligned} \tag{75}$$

$$
\begin{aligned}
&+\{\mathbb{A}\}^{\mathrm{T}} \frac{\partial \int_{\Theta^{\mathrm{a}}} \{\mathbb{B}(\mathbf{x})\}\, d\Theta}{\partial c_{\mathrm{a}}} \{\mathbb{A}\} \Bigg) \{\mathbb{E}^{\mathrm{m}}\} \{\boldsymbol{\varepsilon}^{\mathrm{c}}\} \\
&- \frac{\partial \overline{\mathcal{U}}^{\mathrm{b}}}{\partial c_{\mathrm{a}}} \{\boldsymbol{\varepsilon}^{\mathrm{c}}\}^{\mathrm{T}} \{\mathbb{E}^{\mathrm{m}}\}^{\mathrm{T}} \Bigg(\{\mathbb{A}\}^{\mathrm{T}} \int_{\Theta^{\mathrm{b}}} \{\mathbb{S}^{\mathrm{BF}}(\mathbf{x})\}^{\mathrm{T}}\, d\Theta\, \{\mathbb{L}^{\mathrm{m}}\} + \{\mathbb{L}^{\mathrm{m}}\} \int_{\Theta^{\mathrm{b}}} \{\mathbb{S}^{\mathrm{BF}}(\mathbf{x})\}\, d\Theta\, \{\mathbb{A}\} \\
&+\{\mathbb{A}\}^{\mathrm{T}} \int_{\Theta^{\mathrm{b}}} \{\mathbb{B}(\mathbf{x})\}\, d\Theta\, \{\mathbb{A}\} \Bigg) \{\mathbb{E}^{\mathrm{m}}\} \{\boldsymbol{\varepsilon}^{\mathrm{c}}\} \\
&- \overline{\mathcal{U}}^{\mathrm{b}} \{\boldsymbol{\varepsilon}^{\mathrm{c}}\}^{\mathrm{T}} \{\mathbb{E}^{\mathrm{m}}\}^{\mathrm{T}} \Bigg(\{\mathbb{A}\}^{\mathrm{T}} \frac{\partial \int_{\Theta^{\mathrm{a}}} \{\mathbb{S}^{\mathrm{BF}}(\mathbf{x})\}^{\mathrm{T}}\, d\Theta}{\partial c_{\mathrm{a}}} \{\mathbb{L}^{\mathrm{m}}\} + \{\mathbb{L}^{\mathrm{m}}\} \frac{\partial \int_{\Theta^{\mathrm{b}}} \{\mathbb{S}^{\mathrm{BF}}(\mathbf{x})\}\, d\Theta}{\partial c_{\mathrm{a}}} \{\mathbb{A}\} \\
&+\{\mathbb{A}\}^{\mathrm{T}} \frac{\partial \int_{\Theta^{\mathrm{b}}} \{\mathbb{B}(\mathbf{x})\}\, d\Theta}{\partial c_{\mathrm{a}}} \{\mathbb{A}\} \Bigg) \{\mathbb{E}^{\mathrm{m}}\} \{\boldsymbol{\varepsilon}^{\mathrm{c}}\}
\end{aligned}
\tag{75}
$$

After solving (66) numerically, the optimum c_{a} can be obtained.

4 Numerical Example

This section predicts the optimum volume fractions of inner matrix partition c_{a} for transverse loading problems of the fibrous unitcell by the numerical method presented in Section 3.3, and then the influence functions of elastic strain and eigenstrain are solved analytically through the framework presented in Sections 3.1 and 3.2. The accuracy of the 1 + 2-partition ROH model with predicted c_{a} is verified by comparing it to DNS in this section. Meanwhile, the results of the '1-phase-1-partition' ROH method, denoted as the 1 + 1-partition ROH method in the following part, are also presented to show the improvement of the new partitioning scheme for the ROH method. The honeycomb fibrous unitcell is adopted for DNS, while the results of 1 + 2-partition and 1 + 1-partition ROH methods are obtained from a one-element model that shares the same size as the DNS unitcell. The results of three fiber volume fractions are presented, including 35%, 50%, and 65%. Four Young's moduli E^{m} = 2000, 4000, 6000, 8000 [MPa] and three Poisson's ratios ν^{m} = 0.375, 0.40, 0.425 are chosen to cover the value range of the elastic properties of a matrix of fibrous composite material in engineering. The corresponding relative volume fractions of the inner matrix partition $c_{\mathrm{a}}/c_{\mathrm{m}}$ are exhibited in Fig. 4.

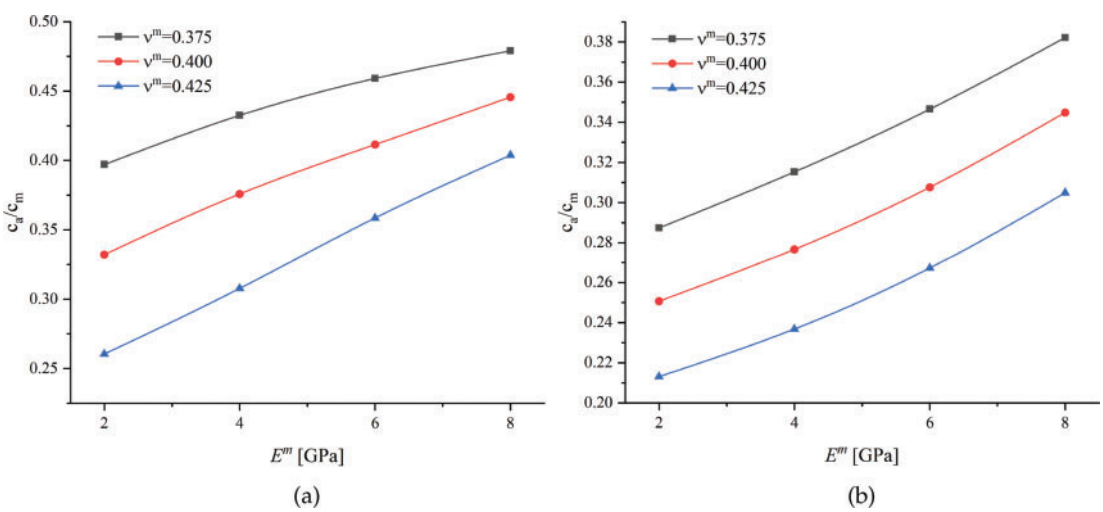

Figure 4: (Continued)

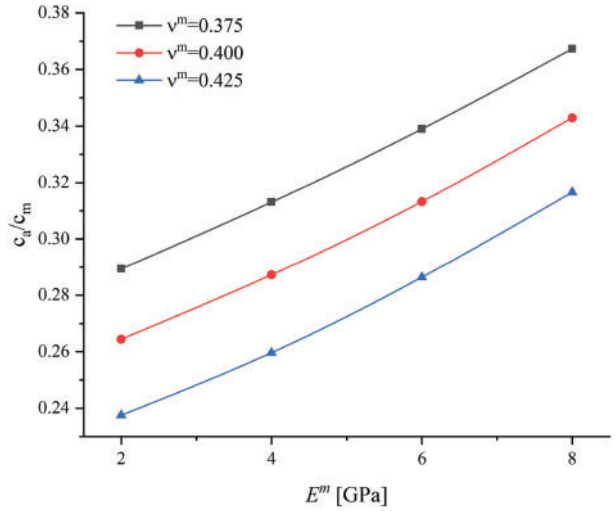

(c)

Figure 4: Numerical relative volume fraction c_a/c_m of different fiber volume fractions: (a) 35%; (b) 50%; (c) 65%

The mechanical fiber properties are given in Table 1. In this section, the yielding and ultimate strength of the matrix phase is 50 [MPa].

Table 1: Elastic properties of fiber

E_a^f	2.51E+02 [GPa]	Young's modulus in axial direction
E_t^f	1.48E+01 [GPa]	Young's modulus in transverse direction
ν_{at}^f	1.50E-02 [−]	Poisson's ratio in axial-transverse plane
ν_t^f	3.00E-01 [−]	Poisson's ratio in the transverse plane
μ_{at}^f	1.50E+04 [−]	shear modulus in axial-transverse plane

4.1 Verification under Transverse Uniaxial Tension Loading

Fig. 5 exhibits that the global response of 1 + 2-partition ROH under transverse uniaxial tension matches well with DNS and perfect plastic yielding can also be reproduced accurately. Figs. 6 and 7 indicate that the matrix phase starts yielding at the inner partition while the outer matrix partition remains elastic; after the outer matrix partition starts yielding, the equivalent plastic strain of the matrix only increases with ε_{22} in the outer partition while equivalent plastic strain in inner matrix partition remains unchanged.

The results of the ultimate strength of the fibrous unitcell under transverse uniaxial tension obtained through DNS, 1 + 2-partition ROH, and 1 + 1-partition ROH are presented in Figs. 8–10. The 1 + 2-partitioning scheme exhibits accuracy superiority compared to the 1 + 1-partition scheme in almost all calculation examples, especially for the cases with high fiber volume fractions. The relative errors of the 1 + 2-partition ROH method are all less than 7.3% and less than 5% in most calculation examples. On the other hand, the strength of the 1 + 1-partition ROH method always tends to be overestimated, which is a typical deficiency of the "1-phase-1-partition" method. The accuracy of 1 + 1-partition ROH is only satisfactory when E^m = 8000 [MPa]. The error expands with the increase of fiber volume fraction and Poisson's ratio of the matrix phase and the reduction of Young's modulus of the matrix phase.

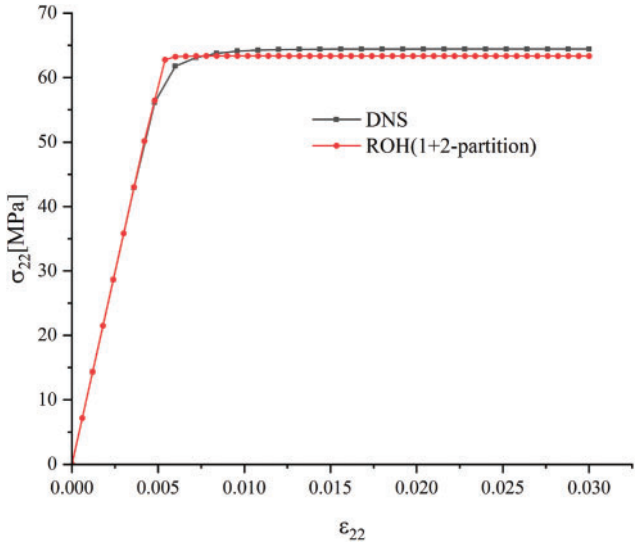

Figure 5: Stress σ_{22} of fibrous unitcell under transverse uniaxial tension: $c^{\mathrm{f}} = 50\%$, $E^{\mathrm{m}} = 8000$ [MPa], $\nu^{\mathrm{m}} = 0.4$

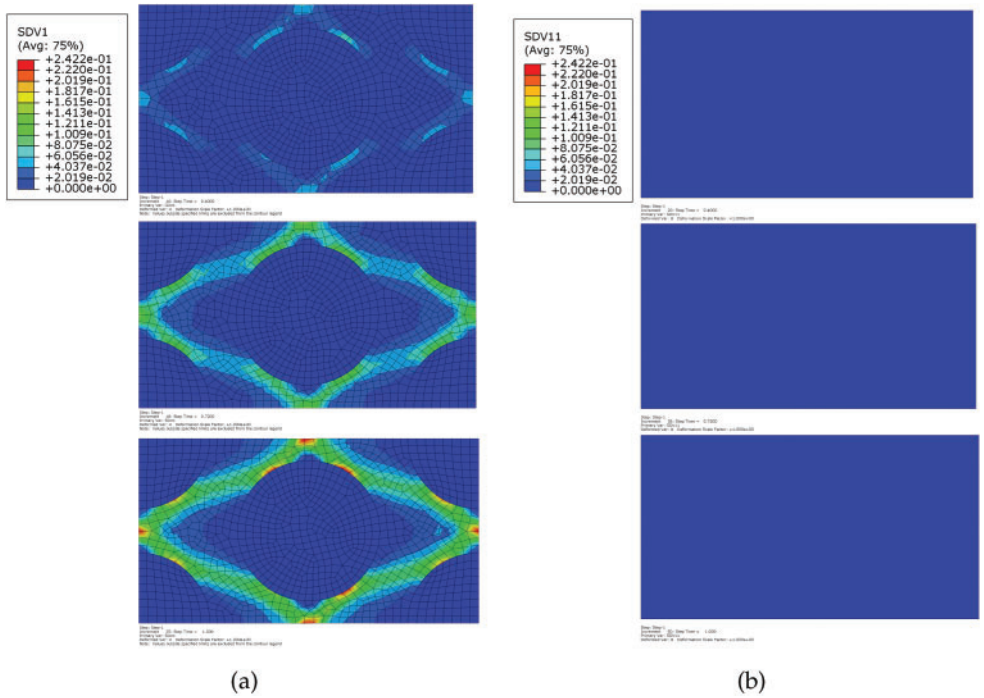

Figure 6: (Continued)

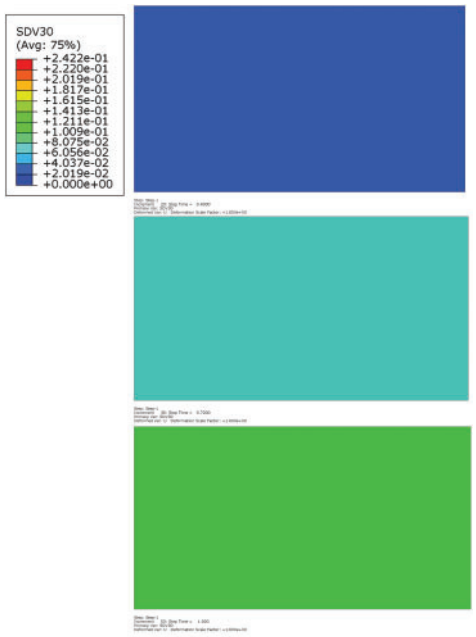

(c)

Figure 6: Comparison of the evolution of equivalent plastic strain in matrix phase under transverse uniaxial tension when the loading is ε_{22} = 0.012, ε_{22} = 0.0216, and ε_{22} = 0.03 and c^{f} = 50%, E^{m} = 8000 [MPa], ν^{m} = 0.4: (a) DNS; (b) Inner matrix partition; (c) Outer matrix partition

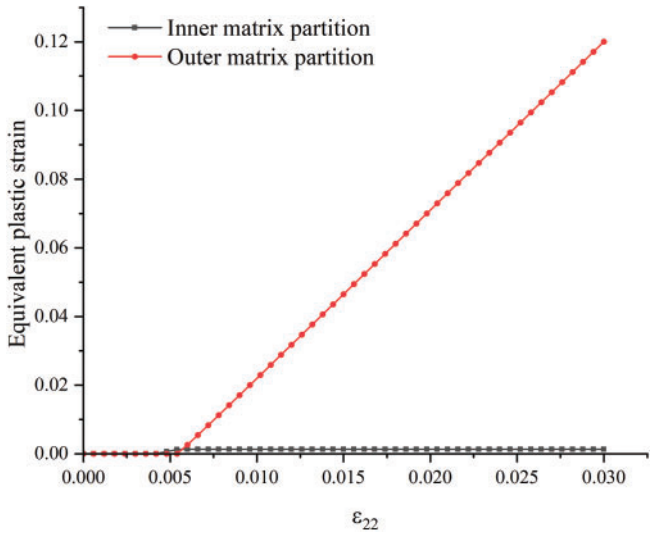

Figure 7: Evolution of equivalent plastic strains at inner and outer matrix partitions under transverse uniaxial tension: c^{f} = 50%, E^{m} = 8000 [MPa], ν^{m} = 0.4

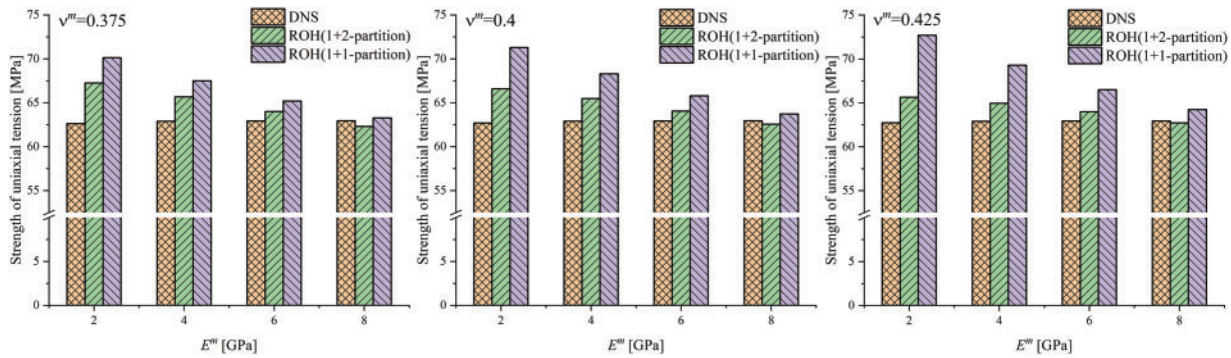

Figure 8: The comparison of ultimate strength of fibrous unitcell under transverse uniaxial tension: c_f = 35%

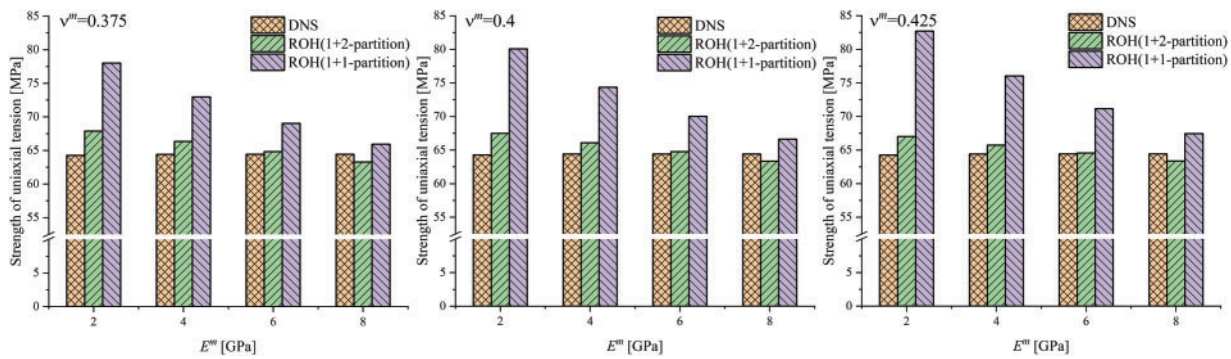

Figure 9: The comparison of ultimate strength of fibrous unitcell under transverse uniaxial tension: c_f = 50%

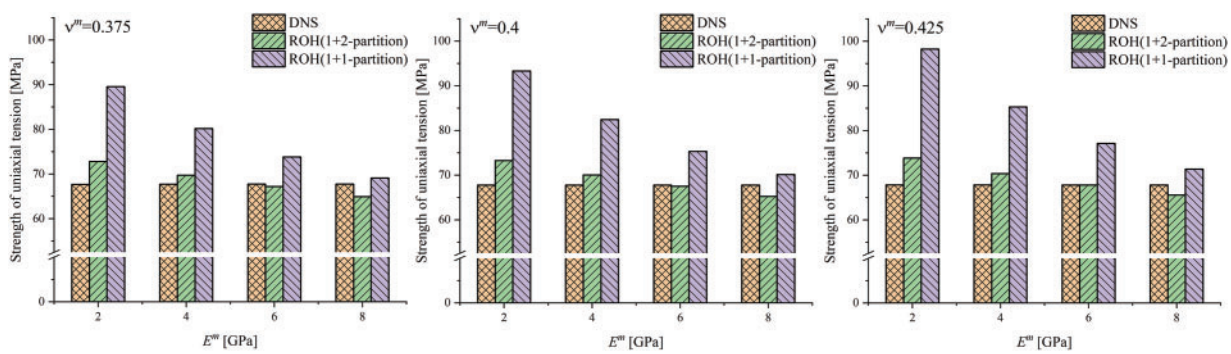

Figure 10: The comparison of ultimate strength of fibrous unitcell under transverse uniaxial tension: c_f = 65%

4.2 Verification under Transverse Shear Loading

Fig. 11 presents the global responses of DNS and 1 + 2-partition ROH under transverse shear. The corresponding evolutions of equivalent plastic strain are given in Figs. 12 and 13. The matrix starts yielding at the interface, and then the yield area expands and grows together. Similarly, the equivalent plastic strain of the inner partition stops increasing soon after the outer partition starts yielding.

The results of ultimate strength are presented in Figs. 14–16. In the transverse shear loading problem, 1 + 2-partition ROH still presents an overall advantage over 1 + 1-partition ROH on calculation accuracy. However, the relative errors are larger than transverse uniaxial tension cases. The largest error is about 20%; in most cases, the error varies within the range of 10%–20%. On the other hand, the accuracy of 1 + 1-partition ROH is unsatisfactory in most cases. Similarly, the strengths of 1 + 1-partition ROH are all overestimated.

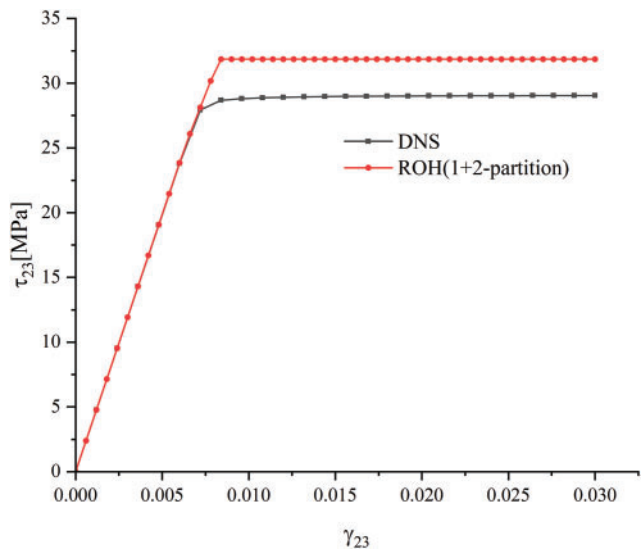

Figure 11: Stress τ_{23} of fibrous unitcell under transverse shear: $c^{\mathrm{f}} = 50\%$, $E^{\mathrm{m}} = 8000$ [MPa], $\nu^{\mathrm{m}} = 0.4$

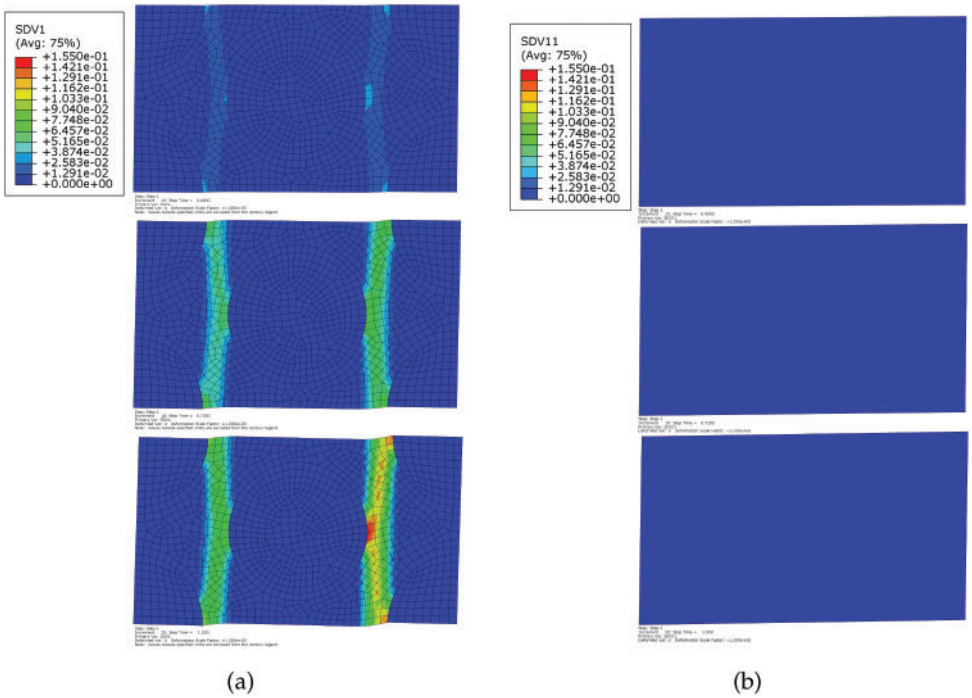

Figure 12: (Continued)

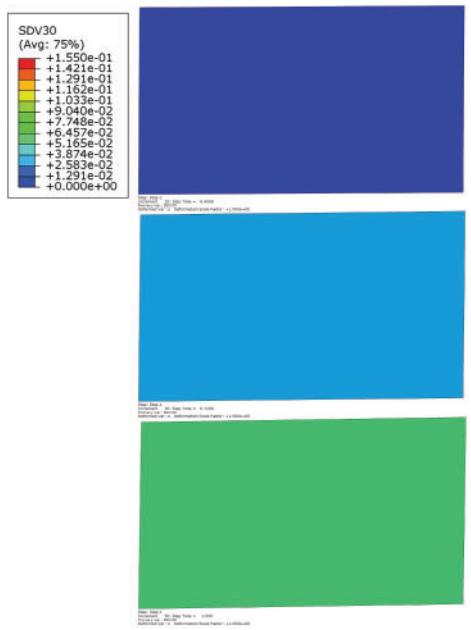

(c)

Figure 12: Comparison of the evolution of equivalent plastic strain in matrix phase under transverse shear when the loading is $\gamma_{23} = 0.012$, $\gamma_{23} = 0.0216$, and $\gamma_{23} = 0.03$ and $c^{\mathrm{f}} = 50\%$, $E^{\mathrm{m}} = 8000$ [MPa], $\nu^{\mathrm{m}} = 0.4$: (a) DNS; (b) Inner matrix partition; (c) Outer matrix partition

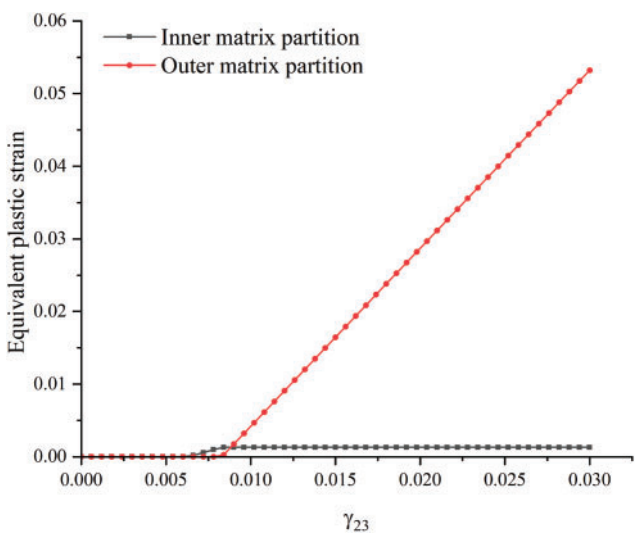

Figure 13: Evolution of equivalent plastic strains at inner and outer matrix partitions under transverse shear: $c^{\mathrm{f}} = 50\%$, $E^{\mathrm{m}} = 8000$ [MPa], $\nu^{\mathrm{m}} = 0.4$

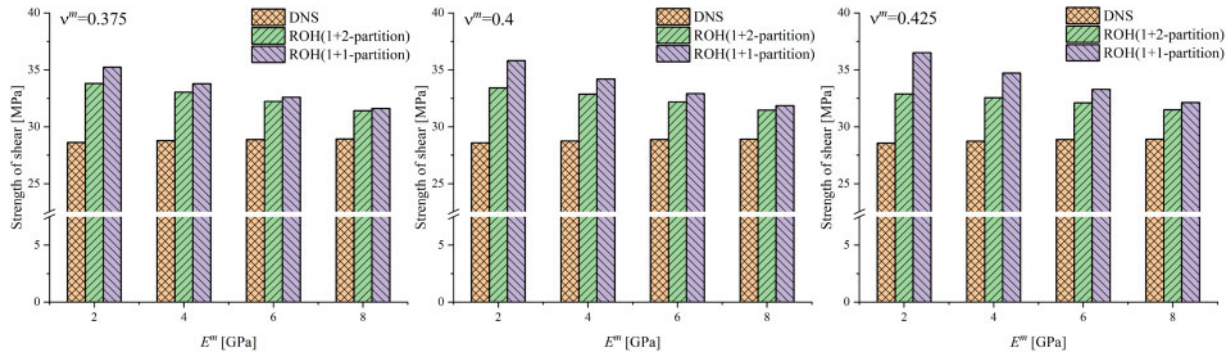

Figure 14: The comparison of ultimate strength of fibrous unitcell under transverse shear: c_f = 35%

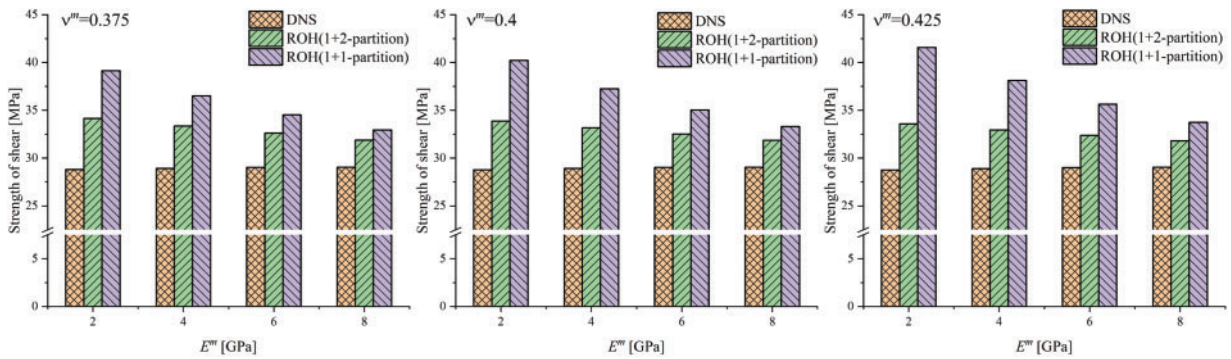

Figure 15: The comparison of ultimate strength of fibrous unitcell under transverse shear: c_f = 50%

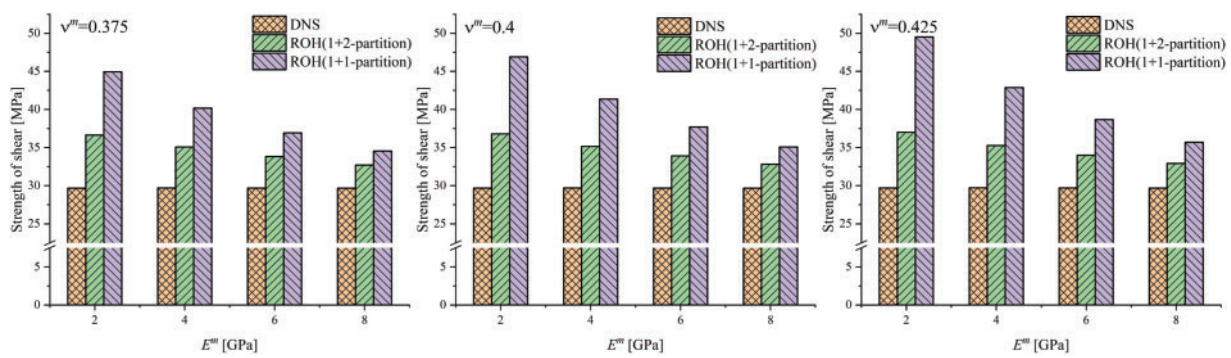

Figure 16: The comparison of ultimate strength of fibrous unitcell under transverse shear: c_f = 65%

5 Discussion

In this study, the 1 + 2-partitioning scheme ROH method shares the same constitutive models of fiber and matrix with the 1 + 1-partition ROH method and DNS. At the expense of an acceptable increase in the internal variables of the overall constitutive model and computation cost, the accuracy of the transverse loading problems of fibrous unitcells improves significantly compared to the typical 1 + 1-partition ROH method [44,47]. In most cases, the relative errors of the 1 + 2 partitioning method are less than 5%

under transverse uniaxial tension and less than 20% under transverse shear loading, demonstrating overall improvement in accuracy compared to the 1 + 1-partition ROH method. Compared to DNS, the computation time of the 1 + 2-partition ROH method is still three orders of magnitude lower. More internal variables or partitions for the ROH method lead to higher fidelity. The 1 + 2-partition ROH method can exhibit more information on the nonlinear evolution process in a single element, as presented in Figs. 6 and 12. The benefit of the switch from 1 + 1-partition to 1 + 2-partition is considerable.

In the ROH method, the number of influence functions to be solved is $M(M+1)$, where M denotes the number of partitions. Increasing the number of partitions will result in a growth in offline stage computation when influence functions are calculated numerically. In addition, finer partitioning leads to smaller character lengths and more degrees of freedom in the mesoscale model. As exhibited in Fig. 17, the number of elements in the unitcell expands significantly as mode partitions are added. For the 1 + 1-partition unitcell, the number of elements is about 300,000; for the 1 + 12-partition unitcell, the value is over 1,500,000, while the thickness of each layered partition is 5% of the fiber radius. The calculation time for influence functions on the offline stage also grows noticeably. Fig. 18 presents the global responses of unitcells calculated by ROH with different partitionings under transverse loadings. Increasing partitions helps the ROH results approach the DNS results, but the accuracy benefits from increasing the number of radial partition layers decrease as the number of partitions grows, and the extra cost of offline and on-line stage computation outweighs the benefits. The proposed analytical solution for influence functions effectively alleviates this issue. The mathematical manipulation of the eigenstrain influence function also visually illustrates the interaction mechanism among the three partitions more visually.

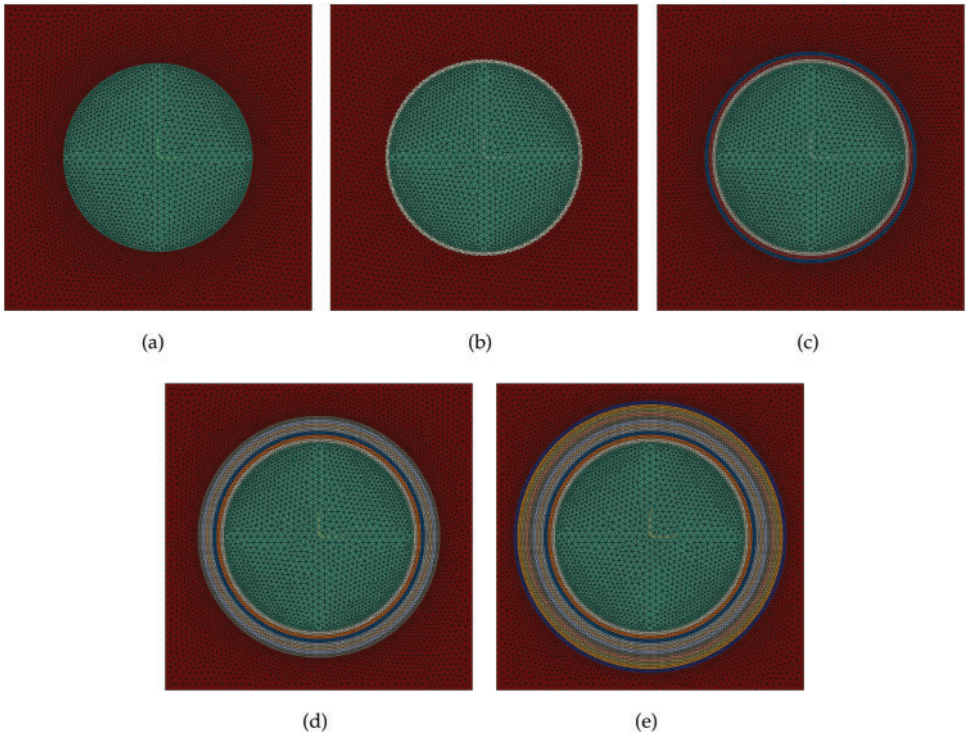

Figure 17: A sketch of fibrous unitcell finite element models with different partitionings (c_f = 30%): (a) 1 + 1-partition; (b) 1 + 2-partition; (c) 1 + 4-partition; (d) 1 + 8-partition; and (e) 1 + 12-partition

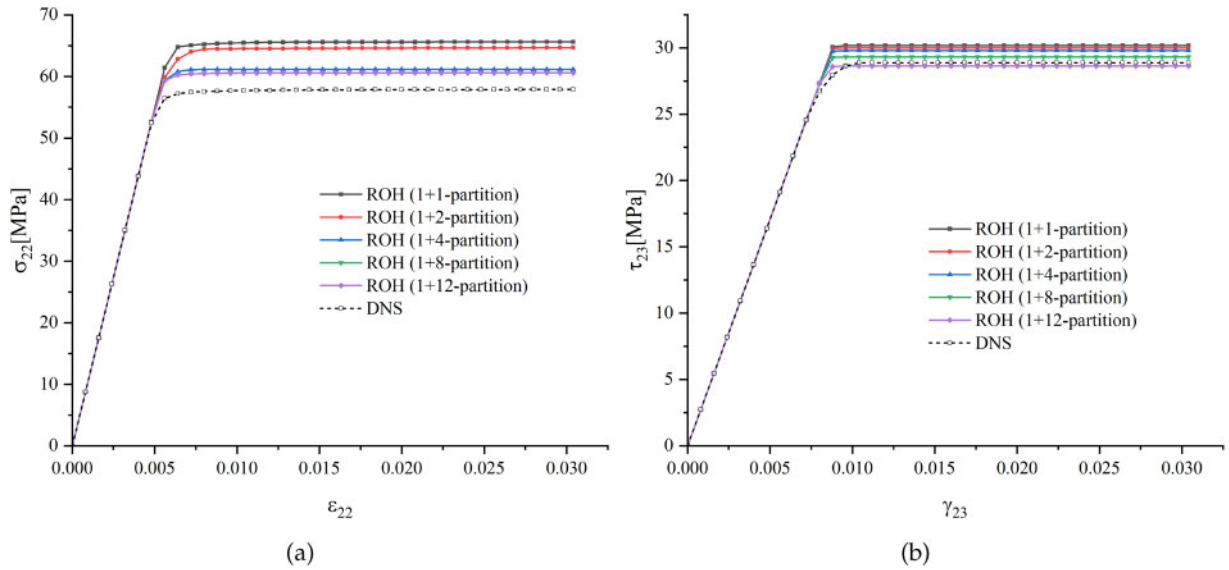

Figure 18: Global responses of fibrous unitcell under transverse loadings of different partitionings with c^{f} = 30%, E^{m} = 8000 [MPa], ν^{m} = 0.4: (a) transverse uniaxial tension; (b) transverse shear

In addition, the influence of partitioning on computational time should also be considered. A beam model with 1000 elements is established and presented in Fig. 19, whose ROH constitutive models are obtained from the unitcells in Fig. 17 to make the impact of the number of partitions more apparent. When the beam is under uniaxial tension along the x-axis, while the longitudinal direction is along the z-axis, Fig. 20 exhibits the variation of computational time with the number of partitions. As the number of partitions increases, the computation time rises significantly. Therefore, it is not advisable to arbitrarily increase the number of partitions. The partitioning strategy for the unitcell should be comprehensively considered to achieve the balance between computation resolution and computation cost, and the proposed partitioning scheme is an ideal solution for fibrous unitcells.

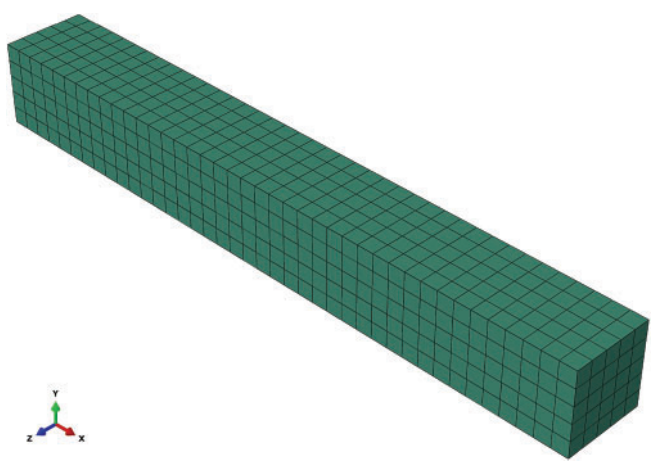

Figure 19: Beam model with multiple elements

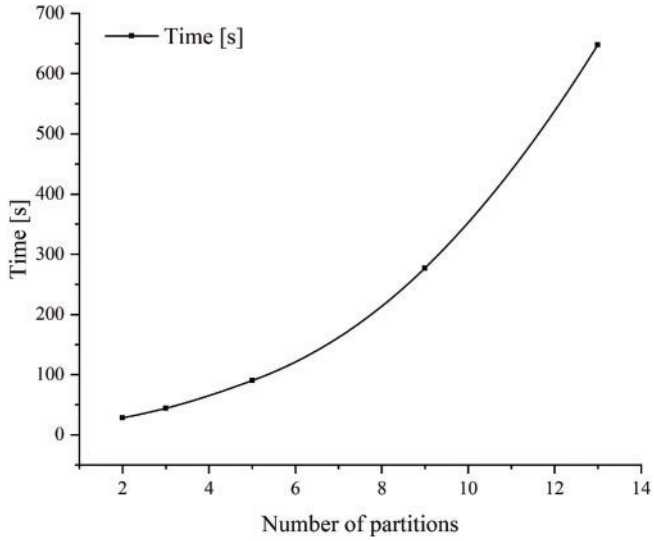

Figure 20: The variation of computation time as the number of partitions increases

The numerical method for determining the inner matrix partition volume fraction is based on a modified Eshelby method for the finite matrix domain. The c_a predicted by this numerical method has demonstrated satisfactory precision for transverse loading cases. In the future, we hope to develop this method further to consider the out-of-plane shear loading pattern so that all the main failure modes of the matrix are involved in this partitioning scheme.

6 Conclusion

This study proposes a new overall constitutive model of the fibrous composite material to provide better accuracy for the simulation of the nonlinear responses. The matrix phase is partitioned into inner and outer partitions to capture the stress concentration within the domain of the matrix phase under transverse loadings, whose optimum volume fraction is decided by a numerical method for minimizing the error of strain energy density compared to an Eshelby method based on finite matrix domain assumption. The nonlinear evolution of the inner and outer matrix partitions are also separated so that the failure mechanism on the mesoscale is exhibited more clearly. In this model, the influence functions of three partitions are calculated by a newly proposed analytical method, which significantly reduces the computation cost of the so-called offline stage compared to the classic numerical method. For example, a rate-independent plasticity model is employed to describe the nonlinear process of the matrix phase, and a series of calculations are conducted to verify the accuracy of the proposed model when simulating the problems under transverse loadings. The accuracy of the results calculated by the new model is satisfactory and superior to that of the 1 + 1-partition ROH method within the value range in the typical application scenario of fibrous composite materials, while the increase of computation cost is limited. As the modified Eshelby method for quantifying the error of strain energy density is limited to transverse load cases, longitudinal shear loading is not involved in the optimization of inner partition volume fractions. This is the primary limitation of the present model and an area to be addressed in future improvement.

Acknowledgement: Financial support by the National Key R&D Program of China and the National Natural Science Foundation of China is gratefully acknowledged. The research is also supported by "The Fundamental Research Funds for the Central Universities, Peking University".

Funding Statement: This work is funded by the National Key R&D Program of China (Grant No. 2023YFA1008901), the National Natural Science Foundation of China (Grant Nos. 11988102, 12172009) and "The Fundamental Research Funds for the Central Universities, Peking University".

Author Contributions: Shanqiao Huang and Zifeng Yuan contributed to the study conceptualization, methodology, data analysis, writing, reviewing and editing. Data collection was performed by Shanqiao Huang. All authors reviewed the results and approved the final version of the manuscript.

Availability of Data and Materials: The data generated through the numerical examples included in this study are available from the corresponding author on request.

Ethics Approval: Not applicable.

Conflicts of Interest: The authors declare no conflicts of interest to report regarding the present study.

Appendix A Proof of the Semi-Positive-Definite Property of $\{\Delta\mathbb{L}\}$

This section studies

$$\{\Delta\mathbb{L}\} \equiv \{\mathbb{L}^{\mathrm{c}}\} - c_{\mathrm{f}} \left\{\mathbb{E}^{\mathrm{f}}\right\}^{\mathrm{T}} \left\{\mathbb{L}^{\mathrm{f}}\right\} \left\{\mathbb{E}^{\mathrm{f}}\right\} - c_{\mathrm{m}} \{\mathbb{E}^{\mathrm{m}}\}^{\mathrm{T}} \{\mathbb{L}^{\mathrm{m}}\} \{\mathbb{E}^{\mathrm{m}}\} \tag{A1}$$

and prove that $\{\Delta\mathbb{L}\}$ is semi-positive-definite. Similarly, decompose $\mathbb{L}^{\mathrm{f}}$ with Cholesky decomposition method into $\left\{\mathbb{L}^{\mathrm{f}}\right\} = \left\{\mathbb{Q}^{\mathrm{f}}\right\}^{\mathrm{T}} \left\{\mathbb{Q}^{\mathrm{f}}\right\}$.

Through the classic linear homogenization process based on asymptotic expansion and perturbation method, the linear homogenized elastic stiffness tensor is given as follows:

$$\mathbb{L}^{\mathrm{c}} = \frac{1}{|\Theta|} \int_{\Theta} \mathbb{E}(\boldsymbol{y}) : \mathbb{L}(\boldsymbol{y}) : \mathbb{E}(\boldsymbol{y}) \, \mathrm{d}\Theta \tag{A2}$$

where $\Theta = \Theta(\boldsymbol{y})$ is the unitcell domain, $\mathbb{E}(\boldsymbol{y})$ is the point-wise elastic strain influence function. $\Theta = \Theta^{\mathrm{f}} \cup \Theta^{\mathrm{m}}$ where Θ^{f} and Θ^{m} denote the fiber and matrix phase domain, respectively. $|\Theta|$ is the volumetric measurement of Θ. Then

$$\mathbb{E}^{\mathrm{f}} = \frac{1}{|\Theta^{\mathrm{f}}|} \int_{\Theta^{\mathrm{f}}} \mathbb{E}(\boldsymbol{y}) \, \mathrm{d}\Theta, \quad \mathbb{E}^{\mathrm{m}} = \frac{1}{|\Theta^{\mathrm{m}}|} \int_{\Theta^{\mathrm{m}}} \mathbb{E}(\boldsymbol{y}) \, \mathrm{d}\Theta \tag{A3}$$

With Voigt notation, (A2) can be rewritten into

$$\{\mathbb{L}^{\mathrm{c}}\} = \frac{1}{|\Theta|} \int_{\Theta^{\mathrm{f}}} \{\mathbb{E}(\boldsymbol{y})\}^{\mathrm{T}} \left\{\mathbb{Q}^{\mathrm{f}}\right\}^{\mathrm{T}} \left\{\mathbb{Q}^{\mathrm{f}}\right\} \{\mathbb{E}(\boldsymbol{y})\} \, \mathrm{d}\Theta + \frac{1}{|\Theta|} \int_{\Theta^{\mathrm{m}}} \{\mathbb{E}(\boldsymbol{y})\}^{\mathrm{T}} \{\mathbb{Q}^{\mathrm{m}}\}^{\mathrm{T}} \{\mathbb{Q}^{\mathrm{m}}\} \{\mathbb{E}(\boldsymbol{y})\} \, \mathrm{d}\Theta \tag{A4}$$

By Cauchy-Schwarz inequality, for arbitrary second-order tensor $\boldsymbol{\eta} = \boldsymbol{\eta}^{\mathrm{T}}$, it can obtain

$$\begin{aligned}
&\frac{1}{|\Theta|} \int_{\Theta^{\mathrm{f}}} \{\boldsymbol{\eta}\}^{\mathrm{T}} \{\mathbb{E}(\boldsymbol{y})\}^{\mathrm{T}} \left\{\mathbb{Q}^{\mathrm{f}}\right\}^{\mathrm{T}} \left\{\mathbb{Q}^{\mathrm{f}}\right\} \{\mathbb{E}(\boldsymbol{y})\} \{\boldsymbol{\eta}\} \, \mathrm{d}\Theta \int_{\Theta^{\mathrm{f}}} 1^2 \, \mathrm{d}\Theta \\
&\geqslant \frac{1}{|\Theta|} \int_{\Theta^{\mathrm{f}}} \{\boldsymbol{\eta}\}^{\mathrm{T}} \{\mathbb{E}(\boldsymbol{y})\}^{\mathrm{T}} \left\{\mathbb{Q}^{\mathrm{f}}\right\}^{\mathrm{T}} \, \mathrm{d}\Theta \int_{\Theta^{\mathrm{f}}} \left\{\mathbb{Q}^{\mathrm{f}}\right\} \{\mathbb{E}(\boldsymbol{y})\} \{\boldsymbol{\eta}\} \, \mathrm{d}\Theta \\
&= \frac{1}{|\Theta|} \int_{\Theta^{\mathrm{f}}} \{\boldsymbol{\eta}\}^{\mathrm{T}} \{\mathbb{E}(\boldsymbol{y})\}^{\mathrm{T}} \, \mathrm{d}\Theta \underbrace{\left\{\mathbb{Q}^{\mathrm{f}}\right\}^{\mathrm{T}} \left\{\mathbb{Q}^{\mathrm{f}}\right\}}_{\{\mathbb{L}^{\mathrm{f}}\}} \int_{\Theta^{\mathrm{f}}} \{\mathbb{E}(\boldsymbol{y})\} \{\boldsymbol{\eta}\} \, \mathrm{d}\Theta = \frac{|\Theta^{\mathrm{f}}|^2}{|\Theta|} \{\boldsymbol{\eta}\}^{\mathrm{T}} \left\{\mathbb{E}^{\mathrm{f}}\right\}^{\mathrm{T}} \left\{\mathbb{L}^{\mathrm{f}}\right\} \left\{\mathbb{E}^{\mathrm{f}}\right\} \{\boldsymbol{\eta}\}
\end{aligned} \tag{A5}$$

Then

$$\{\boldsymbol{\eta}\}^{\mathrm{T}}\left[\frac{1}{|\Theta|}\int_{\Theta^{\mathrm{f}}}\{\mathbb{E}(\boldsymbol{y})\}^{\mathrm{T}}\left\{\mathbb{Q}^{\mathrm{f}}\right\}^{\mathrm{T}}\left\{\mathbb{Q}^{\mathrm{f}}\right\}\{\mathbb{E}(\boldsymbol{y})\}\,\mathrm{d}\Theta-c_{\mathrm{f}}\left\{\mathbb{E}^{\mathrm{f}}\right\}^{\mathrm{T}}\left\{\mathbb{L}^{\mathrm{f}}\right\}\left\{\mathbb{E}^{\mathrm{f}}\right\}\right]\{\boldsymbol{\eta}\}\geqslant 0,\quad \forall\boldsymbol{\eta}=\boldsymbol{\eta}^{\mathrm{T}} \tag{A6}$$

Repeating the same process for the matrix phase yields

$$\{\boldsymbol{\eta}\}^{\mathrm{T}}\left[\{\mathbb{L}^{\mathrm{c}}\}-c_{\mathrm{f}}\left\{\mathbb{E}^{\mathrm{f}}\right\}^{\mathrm{T}}\left\{\mathbb{L}^{\mathrm{f}}\right\}\left\{\mathbb{E}^{\mathrm{f}}\right\}-c_{\mathrm{m}}\{\mathbb{E}^{\mathrm{m}}\}^{\mathrm{T}}\{\mathbb{L}^{\mathrm{m}}\}\{\mathbb{E}^{\mathrm{m}}\}\right]\{\boldsymbol{\eta}\}\geqslant 0,\quad \forall\boldsymbol{\eta}=\boldsymbol{\eta}^{\mathrm{T}} \tag{A7}$$

Appendix B Solution of $\{\mathbb{V}^{\mathrm{m}}\}$ and $\{\mathbb{R}\}$

As the first row and column of $\{\Delta\mathbb{L}\}$ are all zeros, it can be written as follows:

$$\{\Delta\mathbb{L}\}=\begin{bmatrix}0 & \mathbf{0}^{\mathrm{T}}\\ \mathbf{0} & \Delta\boldsymbol{L}\end{bmatrix} \tag{A8}$$

As the first row and column of $\{\Delta\mathbb{E}^{\mathrm{a}}\}$ and $\left\{\Delta\mathbb{E}^{\mathrm{b}}\right\}$ are also zeros, (19) and (20) can be transformed into equations about 5×5 matrices $\Delta\boldsymbol{E}^{\mathrm{a}}$ and $\Delta\boldsymbol{E}^{\mathrm{b}}$. Rewriting $\{\mathbb{L}^{\mathrm{m}}\}$ as follows:

$$\{\mathbb{L}^{\mathrm{m}}\}=\begin{bmatrix}\{\mathbb{L}^{\mathrm{m}}\}_{11} & (\boldsymbol{l}_1^{\mathrm{m}})^{\mathrm{T}}\\ \boldsymbol{l}_1^{\mathrm{m}} & \boldsymbol{L}^{\mathrm{m}}\end{bmatrix} \tag{A9}$$

where $\boldsymbol{L}^{\mathrm{m}}$ is also 5×5 matrix. Then (19) and (20) can be rewritten as following equations about 5×5 matrices:

$$\begin{cases}\Delta\boldsymbol{E}^{\mathrm{a}\,\mathrm{T}}\boldsymbol{L}^{\mathrm{m}}\Delta\boldsymbol{E}^{\mathrm{a}}=\dfrac{c_{\mathrm{b}}/c_{\mathrm{a}}}{c_{\mathrm{a}}+c_{\mathrm{b}}}\Delta\boldsymbol{L}\\ \Delta\boldsymbol{E}^{\mathrm{b}\,\mathrm{T}}\boldsymbol{L}^{\mathrm{m}}\Delta\boldsymbol{E}^{\mathrm{b}}=\dfrac{c_{\mathrm{a}}/c_{\mathrm{b}}}{c_{\mathrm{a}}+c_{\mathrm{b}}}\Delta\boldsymbol{L}\end{cases} \tag{A10}$$

As $\{\Delta\mathbb{L}\}$ is semi-positive-definite real symmetric matrix, $\Delta\boldsymbol{L}$ can be decomposed into $\Delta\boldsymbol{L}=\boldsymbol{V}^{\Delta\,\mathrm{T}}\boldsymbol{\Sigma}\boldsymbol{V}^{\Delta}$ through SVD, where $\boldsymbol{\Sigma}$ is a non-negative diagonal matrix and can be decomposed further $\boldsymbol{\Sigma}=\sqrt{\boldsymbol{\Sigma}}\sqrt{\boldsymbol{\Sigma}}$. Then $\boldsymbol{R}=\sqrt{\boldsymbol{\Sigma}}\boldsymbol{V}^{\Delta}$ and $\sqrt{\boldsymbol{\Sigma}}$ is also a non-negative diagonal matrix. Positive-definite symmetric matrix $\boldsymbol{L}^{\mathrm{m}}$ can also be decomposed by the same way, then

$$\Delta\boldsymbol{L}=\boldsymbol{R}^{\mathrm{T}}\boldsymbol{R} \tag{A11}$$

$$\boldsymbol{L}^{\mathrm{m}}=(\boldsymbol{Q}^{\mathrm{m}})^{\mathrm{T}}\boldsymbol{Q}^{\mathrm{m}} \tag{A12}$$

$\boldsymbol{V}^{\Delta}$, $\boldsymbol{\Sigma}$, $\boldsymbol{R}$ and $\boldsymbol{Q}^{\mathrm{m}}$ are all 5×5 matrices. Substituting (A11) and (A12) into (A10) and relating (17) yields

$$\begin{cases}\boldsymbol{Q}^{\mathrm{m}}\Delta\boldsymbol{E}^{\mathrm{a}}=\sqrt{\dfrac{c_{\mathrm{b}}/c_{\mathrm{a}}}{c_{\mathrm{a}}+c_{\mathrm{b}}}}\boldsymbol{R}\\ \boldsymbol{Q}^{\mathrm{m}}\Delta\boldsymbol{E}^{\mathrm{b}}=-\sqrt{\dfrac{c_{\mathrm{a}}/c_{\mathrm{b}}}{c_{\mathrm{a}}+c_{\mathrm{b}}}}\boldsymbol{R}\end{cases}\quad\Rightarrow\quad\begin{cases}\Delta\boldsymbol{E}^{\mathrm{a}}=\sqrt{\dfrac{c_{\mathrm{b}}/c_{\mathrm{a}}}{c_{\mathrm{a}}+c_{\mathrm{b}}}}(\boldsymbol{Q}^{\mathrm{m}})^{-1}\boldsymbol{R}\\ \Delta\boldsymbol{E}^{\mathrm{b}}=-\sqrt{\dfrac{c_{\mathrm{a}}/c_{\mathrm{b}}}{c_{\mathrm{a}}+c_{\mathrm{b}}}}(\boldsymbol{Q}^{\mathrm{m}})^{-1}\boldsymbol{R}\end{cases} \tag{A13}$$

Then the solutions of $\{\mathbb{V}^{\mathrm{m}}\}$ and $\{\mathbb{R}\}$ are obtained

$$\{\mathbb{V}^{\mathrm{m}}\}=\begin{bmatrix}0 & \mathbf{0}^{\mathrm{T}}\\ \mathbf{0} & (\boldsymbol{Q}^{\mathrm{m}})^{-1}\end{bmatrix}\quad\{\mathbb{R}\}=\begin{bmatrix}0 & \mathbf{0}^{\mathrm{T}}\\ \mathbf{0} & \boldsymbol{R}\end{bmatrix} \tag{A14}$$

The solutions of $\boldsymbol{R}$ and $\boldsymbol{Q}^{\mathrm{m}}$ depend on ordering the singular values in SVD. Due to the transverse isotropy symmetry of fibrous composite materials, the components of $\{\mathbb{E}^{\mathrm{a}}\}$ and $\{\mathbb{E}^{\mathrm{b}}\}$ should satisfy the following equations:

$$\begin{cases} \{\mathbb{E}^{\mathrm{a}}\}_{22} = \{\mathbb{E}^{\mathrm{a}}\}_{33} \\ \{\mathbb{E}^{\mathrm{a}}\}_{23} = \{\mathbb{E}^{\mathrm{a}}\}_{32} \\ \{\mathbb{E}^{\mathrm{a}}\}_{55} = \{\mathbb{E}^{\mathrm{a}}\}_{66} \end{cases} \qquad \begin{cases} \{\mathbb{E}^{\mathrm{b}}\}_{22} = \{\mathbb{E}^{\mathrm{b}}\}_{33} \\ \{\mathbb{E}^{\mathrm{b}}\}_{23} = \{\mathbb{E}^{\mathrm{b}}\}_{32} \\ \{\mathbb{E}^{\mathrm{b}}\}_{55} = \{\mathbb{E}^{\mathrm{b}}\}_{66} \end{cases} \tag{A15}$$

Considering the distribution of non-zeros components in $\Delta\boldsymbol{L}$ and $\boldsymbol{L}^{\mathrm{m}}$, the non-zeros components in $\boldsymbol{R}$ and $\boldsymbol{Q}^{\mathrm{m}}$ can be calculated by following expressions to guarantee the constraints of (A15):

$$\begin{cases} [\boldsymbol{R}]_{11} = [\boldsymbol{R}]_{12} = \sqrt{\dfrac{[\Delta\boldsymbol{L}]_{11} + [\Delta\boldsymbol{L}]_{12}}{2}} \\ [\boldsymbol{R}]_{21} = -[\boldsymbol{R}]_{22} = -\sqrt{\dfrac{[\Delta\boldsymbol{L}]_{11} - [\Delta\boldsymbol{L}]_{12}}{2}} \\ [\boldsymbol{R}]_{kk} = \sqrt{[\Delta\boldsymbol{L}]_{kk}},\ k = 3, 4, 5 \end{cases} \tag{A16}$$

$$\begin{cases} [\boldsymbol{Q}^{\mathrm{m}}]_{11} = [\boldsymbol{Q}^{\mathrm{m}}]_{12} = \sqrt{\dfrac{[\boldsymbol{L}^{\mathrm{m}}]_{11} + [\boldsymbol{L}^{\mathrm{m}}]_{12}}{2}} \\ [\boldsymbol{Q}^{\mathrm{m}}]_{21} = -[\boldsymbol{Q}^{\mathrm{m}}]_{22} = -\sqrt{\dfrac{[\boldsymbol{L}^{\mathrm{m}}]_{11} - [\boldsymbol{L}^{\mathrm{m}}]_{12}}{2}} \\ [\boldsymbol{Q}^{\mathrm{m}}]_{kk} = \sqrt{[\boldsymbol{L}^{\mathrm{m}}]_{kk}},\ k = 3, 4, 5 \end{cases} \tag{A17}$$

After substituting (A16) and (A17) into (A14) and substituting obtained $\{\mathbb{V}^{\mathrm{m}}\}$ and $\{\mathbb{R}\}$ into (25), the derived $\{\mathbb{E}^{\mathrm{a}}\}$ and $\{\mathbb{E}^{\mathrm{b}}\}$ fulfill (A15).

Appendix C Solution of the Axisymmetric Elastic Problem with Bi-Material

Consider that the fiber phase and the inner partition of the matrix phase remain elastic while the second partition loses stiffness. In this case, the fibrous unitcell only has stiffness in the longitudinal direction. This section derives the displacement and strains at the fiber phase and the inner partition of the matrix phase under macroscopic strain $\{\boldsymbol{\varepsilon}^{\mathrm{c}}\} = [1, 0, 0, 0, 0, 0]^{\mathrm{T}}$.

Due to the axisymmetric of the geometry and boundary condition, it only must solve the displacement along the radius direction u_r through the governing equation:

$$\begin{aligned} &\frac{\partial^2 u_r}{\partial r^2} + \frac{1}{r}\frac{\partial u_r}{\partial r} - \frac{u_r}{r^2} + \frac{1}{1 - 2\nu_{\mathrm{at}}^{\mathrm{f}}}\frac{\partial}{\partial r}\left(\frac{\partial u_r}{\partial r} + \frac{u_r}{r}\right) = 0, \quad 0 \leqslant r \leqslant r_{\mathrm{f}} \\ &\frac{\partial^2 u_r}{\partial r^2} + \frac{1}{r}\frac{\partial u_r}{\partial r} - \frac{u_r}{r^2} + \frac{1}{1 - 2\nu^{\mathrm{m}}}\frac{\partial}{\partial r}\left(\frac{\partial u_r}{\partial r} + \frac{u_r}{r}\right) = 0, \quad r_{\mathrm{f}} < r \leqslant r_{\mathrm{f}} + t_{\mathrm{a}} \equiv r_{\mathrm{a}} \end{aligned} \tag{A18}$$

with continuity condition for the displacement u_r and the stress ε_{rr} at $r = r_{\mathrm{f}}$ that

$$u_r|_{r \to r_{\mathrm{f}}^-} = u_r|_{r \to r_{\mathrm{f}}^+} \tag{A19}$$

and

$$\begin{aligned}&\frac{E_{\mathrm{t}}^{\mathrm{f}}}{(1+\nu_{\mathrm{t}}^{\mathrm{f}})(1-\nu_{\mathrm{t}}^{\mathrm{f}}-2\nu_{\mathrm{at}}^{\mathrm{f}}\nu_{\mathrm{ta}}^{\mathrm{f}})}\left[(1-\nu_{\mathrm{at}}^{\mathrm{f}}\nu_{\mathrm{ta}}^{\mathrm{f}})\frac{\partial u_r}{\partial r}+(\nu_{\mathrm{t}}^{\mathrm{f}}+\nu_{\mathrm{at}}^{\mathrm{f}}\nu_{\mathrm{ta}}^{\mathrm{f}})\frac{u_r}{r}+\nu_{\mathrm{at}}^{\mathrm{f}}(1+\nu_{\mathrm{t}}^{\mathrm{f}})\right]_{r\to r_{\mathrm{f}}^{-}}\\&=\frac{E^{\mathrm{m}}}{(1+\nu^{\mathrm{m}})(1-2\nu^{\mathrm{m}})}\left[(1-\nu^{\mathrm{m}})\frac{\partial u_r}{\partial r}+\nu^{\mathrm{m}}\frac{u_r}{r}+\nu^{\mathrm{m}}\right]_{r\to r_{\mathrm{f}}^{+}}\end{aligned}\tag{A20}$$

respectively. In addition, it requires the traction-free boundary condition at $r = r_{\mathrm{a}}$ that

$$\frac{E^{\mathrm{m}}}{(1+\nu^{\mathrm{m}})(1-2\nu^{\mathrm{m}})}\left[(1-\nu^{\mathrm{m}})\frac{\partial u_r}{\partial r}+\nu^{\mathrm{m}}\frac{u_r}{r}+\nu^{\mathrm{m}}\right]_{r=r_{\mathrm{a}}}=0\tag{A21}$$

r_{f} is the radius of the fiber, t_{a} is the thickness of the inner partition of the matrix phase.

The radii r_{f} and r_{a} are related with volume fraction c_{f} and c_{a} that

$$c_{\mathrm{f}}=\pi r_{\mathrm{f}}^2,\ c_{\mathrm{a}}=\pi(r_{\mathrm{a}}^2-r_{\mathrm{f}}^2)\tag{A22}$$

with the area of the transverse cross-section of the unitcell is 1, so that

$$c_{\mathrm{b}}=1-c_{\mathrm{f}}-c_{\mathrm{a}}=1-\pi r_{\mathrm{a}}^2\tag{A23}$$

A piecewise function of u_r can be derived that

$$u_r=\begin{cases}C_1 r, & 0\leqslant r\leqslant r_{\mathrm{f}}\\ C_2 r+\dfrac{C_3}{r}, & r_{\mathrm{f}}\leqslant r\leqslant r_{\mathrm{a}}\end{cases}\tag{A24}$$

with C_i, $i = 1, 2, 3$ are the constants to be determined by the boundary condition and continuity conditions that

$$\begin{cases}(C_1+\nu_{\mathrm{at}}^{\mathrm{f}})-(C_2+\nu^{\mathrm{m}})-\dfrac{C_3}{r_{\mathrm{f}}^2}=\nu_{\mathrm{at}}^{\mathrm{f}}-\nu^{\mathrm{m}}\\ \dfrac{E_{\mathrm{t}}^{\mathrm{f}}}{1-\nu_{\mathrm{t}}^{\mathrm{f}}-2\nu_{\mathrm{at}}^{\mathrm{f}}\nu_{\mathrm{ta}}^{\mathrm{f}}}(C_1+\nu_{\mathrm{at}}^{\mathrm{f}})-\dfrac{E^{\mathrm{m}}}{(1+\nu^{\mathrm{m}})(1-2\nu^{\mathrm{m}})}(C_2+\nu^{\mathrm{m}})+\dfrac{E^{\mathrm{m}}}{1+\nu^{\mathrm{m}}}\dfrac{C_3}{r_{\mathrm{f}}^2}=0\\ (C_2+\nu^{\mathrm{m}})-(1-2\nu^{\mathrm{m}})\dfrac{C_3}{r_{\mathrm{a}}^2}=0\end{cases}\tag{A25}$$

which gives

$$\begin{cases}C_1=-\dfrac{c_{\mathrm{a}}\varphi(1-2\nu^{\mathrm{m}})(\nu^{\mathrm{m}}-\nu_{\mathrm{at}}^{\mathrm{f}})}{2c_{\mathrm{f}}(1-\nu^{\mathrm{m}})+c_{\mathrm{a}}(1+\varphi(1-2\nu^{\mathrm{m}}))}-\nu_{\mathrm{at}}^{\mathrm{f}}\\ C_2=\dfrac{c_{\mathrm{f}}(1-2\nu^{\mathrm{m}})(\nu^{\mathrm{m}}-\nu_{\mathrm{at}}^{\mathrm{f}})}{2c_{\mathrm{f}}(1-\nu^{\mathrm{m}})+c_{\mathrm{a}}(1+\varphi(1-2\nu^{\mathrm{m}}))}-\nu^{\mathrm{m}}\\ C_3=\dfrac{(c_{\mathrm{f}}+c_{\mathrm{a}})(\nu^{\mathrm{m}}-\nu_{\mathrm{at}}^{\mathrm{f}})}{2c_{\mathrm{f}}(1-\nu^{\mathrm{m}})+c_{\mathrm{a}}(1+\varphi(1-2\nu^{\mathrm{m}}))}r_{\mathrm{f}}^2\end{cases}\tag{A26}$$

with non-dimensional constant

$$\varphi\equiv\frac{E^{\mathrm{m}}}{(1+\nu^{\mathrm{m}})(1-2\nu^{\mathrm{m}})}\bigg/\left(\frac{E_{\mathrm{t}}^{\mathrm{f}}}{1-\nu_{\mathrm{t}}^{\mathrm{f}}-2\nu_{\mathrm{at}}^{\mathrm{f}}\nu_{\mathrm{ta}}^{\mathrm{f}}}\right)\tag{A27}$$

φ is the ratio of the transverse bulk modulus of the matrix phase with respect to the fiber phase. Thus $\varphi = (\lambda^{\mathrm{m}} + \mu^{\mathrm{m}})/k^{\mathrm{f}}$, with k^{f} the HILL's constant representing the transverse bulk modulus for the fiber phase, and λ^{m} and μ^{m} the LAMÉ constant for the matrix phase.

Accordingly, within the fiber phase, the normal strain along the radius direction gives

$$\varepsilon_{rr}^{\mathrm{f}} = \frac{\partial u_r}{\partial r} = C_1 = -\frac{c_{\mathrm{a}}\varphi(1-2\nu^{\mathrm{m}})(\nu^{\mathrm{m}} - \nu_{\mathrm{at}}^{\mathrm{f}})}{2c_{\mathrm{f}}(1-\nu^{\mathrm{m}}) + c_{\mathrm{a}}(1+\varphi(1-2\nu^{\mathrm{m}}))} - \nu_{\mathrm{at}}^{\mathrm{f}} \tag{A28}$$

and for the matrix phase,

$$\varepsilon_{rr}^{\mathrm{m}} = \frac{\partial u_r}{\partial r} = C_2 - \frac{C_3}{r^2} = -\nu^{\mathrm{m}} + \frac{\nu^{\mathrm{m}} - \nu_{\mathrm{at}}^{\mathrm{f}}}{2c_{\mathrm{f}}(1-\nu^{\mathrm{m}}) + c_{\mathrm{a}}(1+\varphi(1-2\nu^{\mathrm{m}}))}\left[c_{\mathrm{f}}(1-2\nu^{\mathrm{m}}) - (c_{\mathrm{f}} + c_{\mathrm{a}})\frac{r_{\mathrm{f}}^2}{r^2}\right] \tag{A29}$$

The averaged normal strain along the radius direction for the inner partition of the matrix phase gives

$$\begin{aligned}\bar{\varepsilon}_{rr}^{\mathrm{a}} &\equiv \frac{1}{\pi(r_{\mathrm{a}}^2 - r_{\mathrm{f}}^2)}2\pi\int_{r_{\mathrm{f}}}^{r_{\mathrm{a}}} \varepsilon_{rr}^{\mathrm{a}} r\,\mathrm{d}r = \frac{1}{\pi(r_{\mathrm{a}}^2 - r_{\mathrm{f}}^2)}2\pi\int_{r_{\mathrm{f}}}^{r_{\mathrm{a}}}\left(C_2 - \frac{C_3}{r^2}\right) r\,\mathrm{d}r \\ &= -\nu^{\mathrm{m}} + \frac{\nu^{\mathrm{m}} - \nu_{\mathrm{at}}^{\mathrm{f}}}{2c_{\mathrm{f}}(1-\nu^{\mathrm{m}}) + c_{\mathrm{a}}(1+\varphi(1-2\nu^{\mathrm{m}}))}\left[c_{\mathrm{f}}(1-2\nu^{\mathrm{m}}) - \frac{c_{\mathrm{f}}}{c_{\mathrm{a}}}\ln\frac{c_{\mathrm{f}} + c_{\mathrm{a}}}{c_{\mathrm{f}}}\right]\end{aligned} \tag{A30}$$

Appendix D Expression of Eshelby Tensors for Cylindrical Inclusion within Finite Matrix Domain

Based on the work by Ma et al. [48], the expressions of non-zero components of Eshelby tensors for a cylindrical inclusion in a finite elastic matrix are given in the following part. In these expressions, $i, j, k, l = 2, 3$ and $x_2^0 = \cos\theta$, $x_3^0 = \sin\theta$, and r_{f} is the radius of the fiber. The axis of the fiber is the axis of cylindrical coordinates.

$$\begin{cases} S_{ijkl}^{\mathrm{f}} = \dfrac{4\nu^{\mathrm{m}} - 1}{8(1-\nu^{\mathrm{m}})}\delta_{ij}\delta_{kl} + \dfrac{3 - 4\nu^{\mathrm{m}}}{8(1-\nu^{\mathrm{m}})}(\delta_{ik}\delta_{jl} + \delta_{il}\delta_{jk}) \\ S_{i1j1}^{\mathrm{f}} = \dfrac{1}{4}\delta_{ij} \\ S_{ij11}^{\mathrm{f}} = \dfrac{\nu^{\mathrm{m}}}{2(1-\nu^{\mathrm{m}})}\delta_{ij} \end{cases} \tag{A31}$$

$$\begin{cases} S_{ijkl}^{\mathrm{m}}(r,\theta) = \dfrac{r_{\mathrm{f}}^2}{8(1-\nu^{\mathrm{m}})r^4}\Big[(4\nu^{\mathrm{m}}r^2 - 2r^2 + r_{\mathrm{f}}^2)\delta_{ij}\delta_{kl} + (-4\nu^{\mathrm{m}}r^2 + 2r^2 + r_{\mathrm{f}}^2)(\delta_{ik}\delta_{jl} + \delta_{il}\delta_{jk}) \\ \qquad - (2\nu^{\mathrm{m}}r^2 - r^2 + r_{\mathrm{f}}^2)\delta_{kl}x_i^0x_j^0 + 4(r^2 - r_{\mathrm{f}}^2)\delta_{ij}x_k^0x_l^0 \\ \qquad +4(\nu^{\mathrm{m}}r^2 - r_{\mathrm{f}}^2)(\delta_{ik}x_j^0x_l^0 + \delta_{il}x_j^0x_k^0 + \delta_{jk}x_i^0x_l^0 + \delta_{jl}x_i^0x_k^0) + 8(3r_{\mathrm{f}}^2 - 2r^2)x_i^0x_j^0x_k^0x_l^0\Big] \\ S_{i1j1}^{\mathrm{m}}(r,\theta) = \dfrac{r_{\mathrm{f}}^2}{4r^2}(\delta_{ij} - 2x_i^0x_j^0) \\ S_{ij11}^{\mathrm{m}}(r,\theta) = \dfrac{\nu^{\mathrm{m}}r_{\mathrm{f}}^2}{2(1-\nu^{\mathrm{m}})r^2}(\delta_{ij} - 2x_i^0x_j^0) \end{cases} \tag{A32}$$

$$
\begin{cases}
S_{2222}^{\mathbf{BF}}(r,\theta) = -\dfrac{c_{\mathrm{f}}\left[6c_{\mathrm{f}}^2 r^2 - 3c_{\mathrm{f}}\left(2r^2 + r_{\mathrm{f}}^2\right) + 6(c_{\mathrm{f}}-1)c_{\mathrm{f}} r^2 (2\nu^{\mathrm{m}}-1)\cos 2\theta + 2r_{\mathrm{f}}^2\left(8(\nu^{\mathrm{m}})^2 - 16\nu^{\mathrm{m}} + 9\right)\right]}{8r_{\mathrm{f}}^2\left[4(\nu^{\mathrm{m}})^2 - 7\nu^{\mathrm{m}} + 3\right]} \\
S_{2233}^{\mathbf{BF}}(r,\theta) = \dfrac{c_{\mathrm{f}}\left[6c_{\mathrm{f}}^2 r^2 - 3c_{\mathrm{f}}\left(2r^2 + r_{\mathrm{f}}^2\right) + 6(c_{\mathrm{f}}-1)c_{\mathrm{f}} r^2 (2\nu^{\mathrm{m}}-1)\cos 2\theta + 2r_{\mathrm{f}}^2\left(8(\nu^{\mathrm{m}})^2 - 8\nu^{\mathrm{m}} + 3\right)\right]}{8r_{\mathrm{f}}^2\left[4(\nu^{\mathrm{m}})^2 - 7\nu^{\mathrm{m}} + 3\right]} \\
S_{3322}^{\mathbf{BF}}(r,\theta) = -\dfrac{c_{\mathrm{f}}\left[-6c_{\mathrm{f}}^2 r^2 + 3c_{\mathrm{f}}\left(2r^2 + r_{\mathrm{f}}^2\right) + 6(c_{\mathrm{f}}-1)c_{\mathrm{f}} r^2 (2\nu^{\mathrm{m}}-1)\cos 2\theta - 2r_{\mathrm{f}}^2\left(8(\nu^{\mathrm{m}})^2 - 8\nu^{\mathrm{m}} + 3\right)\right]}{8r_{\mathrm{f}}^2\left[4(\nu^{\mathrm{m}})^2 - 7\nu^{\mathrm{m}} + 3\right]} \\
S_{3333}^{\mathbf{BF}}(r,\theta) = \dfrac{c_{\mathrm{f}}\left[-6c_{\mathrm{f}}^2 r^2 + 3c_{\mathrm{f}}\left(2r^2 + r_{\mathrm{f}}^2\right) + 6(c_{\mathrm{f}}-1)c_{\mathrm{f}} r^2 (2\nu^{\mathrm{m}}-1)\cos 2\theta - 2r_{\mathrm{f}}^2\left(8(\nu^{\mathrm{m}})^2 - 16\nu^{\mathrm{m}} + 9\right)\right]}{8r_{\mathrm{f}}^2\left[4(\nu^{\mathrm{m}})^2 - 7\nu^{\mathrm{m}} + 3\right]} \\
S_{2223}^{\mathbf{BF}}(r,\theta) = S_{3323}^{\mathbf{BF}}(r,\theta) = -\dfrac{3(c_{\mathrm{f}}-1)c_{\mathrm{f}}^2 r^2 \sin 2\theta (2\nu^{\mathrm{m}}-1)}{4r_{\mathrm{f}}^2\left[4(\nu^{\mathrm{m}})^2 - 7\nu^{\mathrm{m}} + 3\right]} \\
S_{2323}^{\mathbf{BF}}(r,\theta) = -\dfrac{c_{\mathrm{f}}\left[6c_{\mathrm{f}}^2 r^2 - 3c_{\mathrm{f}}\left(2r^2 + r_{\mathrm{f}}^2\right) + 4r_{\mathrm{f}}^2\left(4(\nu^{\mathrm{m}})^2 - 6\nu^{\mathrm{m}} + 3\right)\right]}{8r_{\mathrm{f}}^2\left[4(\nu^{\mathrm{m}})^2 - 7\nu^{\mathrm{m}} + 3\right]}
\end{cases}
\tag{A33}
$$

References

1. Fish J, Wagner GJ, Keten S. Mesoscopic and multiscale modelling in materials. Nat Mat. 2021;20(6):774–86. doi:10.1038/s41563-020-00913-0.
2. Guo Z, Hou Z, Tian X, Zhu W, Wang C, Luo M, et al. 3D printing of curvilinear fiber reinforced variable stiffness composite structures: a review. Compos Part B: Eng. 2025;291(1):112039. doi:10.1016/j.compositesb.2024.112039.
3. Li Z, Wang B, Hao P, Du K, Mao Z, Li T. Multi-scale numerical calculations for the interphase mechanical properties of carbon fiber reinforced thermoplastic composites. Compos Sci Technol. 2025;260:110982. doi:10.1016/j.compscitech.2024.110982.
4. Hashin Z. Failure criteria for unidirectional fiber composites. J Appl Mech. 1980 Jun;47(2):329–34. doi:10.1115/1.3153664.
5. Chow CL, Wang J. An anisotropic theory of elasticity for continuum damage mechanics. Int J Fract. 1987;33(1):3–16. doi:10.1007/BF00034895.
6. Camanho P, Bessa M, Catalanotti G, Vogler M, Rolfes R. Modeling the inelastic deformation and fracture of polymer composites-Part II: smeared crack model. Mech Mat. 2013;59:36–49. doi:10.1016/j.mechmat.2012.12.001.
7. Canal LP, Segurado J, Llorca J. Failure surface of epoxy-modified fiber-reinforced composites under transverse tension and out-of-plane shear. Int J Sol Struct. 2009;46(11):2265–74. doi:10.1016/j.ijsolstr.2009.01.014.
8. Ha SK, Jin KK, Huang Y. Micro-mechanics of Failure (MMF) for continuous fiber reinforced composites. J Compos Mat. 2008;42(18):1873–95. doi:10.1177/0021998308093911.
9. Lomov SV, Ivanov DS, Verpoest I, Zako M, Kurashiki T, Nakai H, et al. Meso-FE modelling of textile composites: road map, data flow and algorithms. Compos Sci Technol. 2007;67(9):1870–91. doi:10.1016/j.compscitech.2006.10.017.
10. Zhi J, Poh LH, Tay TE, Tan VBC. Direct FE2 modeling of heterogeneous materials with a micromorphic computational homogenization framework. Comput Methods Appl Mech Eng. 2022;393(1):114837. doi:10.1016/j.cma.2022.114837.
11. Yuan Z, Fish J. Toward realization of computational homogenization in practice. Int J Num Meth Eng. 2008;73(3):361–80. doi:10.1002/nme.2074.
12. Kouznetsova V, Geers MG, Brekelmans WM. Multi-scale constitutive modelling of heterogeneous materials with a gradient-enhanced computational homogenization scheme. Int J Num Meth Eng. 2002;54(8):1235–60. doi:10.1002/nme.541.

13. Dvorak GJ. Transformation field analysis of inelastic composite materials. Proc Royal Soc London Ser A: Mathem Phys Sci. 1992;437(1900):311–27.
14. Dvorak GJ, Benveniste Y. On transformation strains and uniform fields in multiphase elastic media. Proc Royal Soc London Ser A: Mathem Phys Sci. 1992;437(1900):291–310.
15. Ng ET, Suleman A. Implicit stress integration in elastoplasticity of n-phase fiber-reinforced composites. Mech Adv Mat Struct. 2007;14(8):633–41. doi:10.1080/15376490701672302.
16. Khattab IA, Sinapius M. Multiscale modelling and simulation of polymer nanocomposites using transformation field analysis (TFA). Compos Struct. 2019;209:981–91. doi:10.1016/j.compstruct.2018.10.100.
17. Castrogiovanni A, Marfia S, Auricchio F, Sacco E. TFA and HS based homogenization techniques for nonlinear composites. Int J Solids Struct. 2021;225(3):111050. doi:10.1016/j.ijsolstr.2021.111050.
18. Kanouté P, Boso D, Chaboche JL, Schrefler B. Multiscale methods for composites: a review. Arch Computat Meth Eng. 2009;16(1):31–75. doi:10.1007/s11831-008-9028-8.
19. Wang Y, Huang Z. Analytical micromechanics models for elastoplastic behavior of long fibrous composites: a critical review and comparative study. Materials. 2018;11(10):1919. doi:10.3390/ma11101919.
20. Spilker K, Nguyen VD, Adam L, Wu L, Noels L. Piecewise-uniform homogenization of heterogeneous composites using a spatial decomposition based on inelastic micromechanics. Compos Struct. 2022;295(3):115836. doi:10.1016/j.compstruct.2022.115836.
21. Michel JC, Suquet P. Computational analysis of nonlinear composite structures using the nonuniform transformation field analysis. Comput Methods Appl Mech Eng. 2004;193(48–51):5477–502. doi:10.1016/j.cma.2003.12.071.
22. Ju X, Mahnken R, Xu Y, Liang L. NTFA-enabled goal-oriented adaptive space-time finite elements for micro-heterogeneous elastoplasticity problems. Comput Methods Appl Mech Eng. 2022;398(11):115199. doi:10.1016/j.cma.2022.115199.
23. Liu Z, Bessa M, Liu WK. Self-consistent clustering analysis: an efficient multi-scale scheme for inelastic heterogeneous materials. Comput Meth Appl Mech Eng. 2016;306(1):319–41. doi:10.1016/j.cma.2016.04.004.
24. Kafka OL, Yu C, Shakoor M, Liu Z, Wagner GJ, Liu WK. Data-driven mechanistic modeling of influence of microstructure on high-cycle fatigue life of nickel titanium. JOM. 2018;70(7):1154–8. doi:10.1007/s11837-018-2868-2.
25. Liu Z, Fleming M, Liu WK. Microstructural material database for self-consistent clustering analysis of elastoplastic strain softening materials. Comput Meth Appl Mech Eng. 2018;330(41):547–77. doi:10.1016/j.cma.2017.11.005.
26. Liu Z, Kafka OL, Yu C, Liu WK. Data-driven self-consistent clustering analysis of heterogeneous materials with crystal plasticity. In: Computational methods in applied sciences. Cham: Springer International Publishing; 2018. Vol. 46, p. 221–42.
27. Yu C, Kafka OL, Liu WK. Self-consistent clustering analysis for multiscale modeling at finite strains. Comput Meth Appl Mech Eng. 2019;349(5330):339–59. doi:10.1016/j.cma.2019.02.027.
28. Zhang L, Tang S. Displacement reconstruction and strain refinement of clustering-based homogenization. Theor Appl Mech Lett. 2021;11(6):100285. doi:10.1016/j.taml.2021.100285.
29. Tang S, Zhu X. Clustering solver for displacement-based numerical homogenization. Theor Appl Mech Lett. 2022;12(3):100306. doi:10.1016/j.taml.2021.100306.
30. Ri JH, Hong HS, Ri SG. Cluster based nonuniform transformation field analysis: an efficient homogenization for inelastic heterogeneous materials. Int J Num Meth Eng. 2021;122(17):4458–85. doi:10.1002/nme.6696.
31. Ri JH, Ri UI, Hong HS. Multiscale analysis of elastic-viscoplastic composite using a cluster-based reduced-order model. Compos Struct. 2021;272:114209. doi:10.1016/j.compstruct.2021.114209.
32. Tang S, Zhang L, Liu WK. From virtual clustering analysis to self-consistent clustering analysis: a mathematical study. Computat Mech. 2018;62(6):1443–60. doi:10.1007/s00466-018-1573-x.
33. Cheng G, Li X, Nie Y, Li H. FEM-Cluster based reduction method for efficient numerical prediction of effective properties of heterogeneous material in nonlinear range. Comput Meth Appl Mech Eng. 2019;348:157–84. doi:10.1016/j.cma.2019.01.019.

34. Bessa MA, Bostanabad R, Liu Z, Hu A, Apley DW, Brinson C, et al. A framework for data-driven analysis of materials under uncertainty: countering the curse of dimensionality. Comput Meth Appl Mech Eng. 2017;320(1):633–67. doi:10.1016/j.cma.2017.03.037.
35. Han X, Xu C, Xie W, Meng S. Multiscale computational homogenization of woven composites from microscale to mesoscale using data-driven self-consistent clustering analysis. Compos Struct. 2019;220:760–8. doi:10.1016/j.compstruct.2019.03.053.
36. Li H, Kafka OL, Gao J, Yu C, Nie Y, Zhang L, et al. Clustering discretization methods for generation of material performance databases in machine learning and design optimization. Comput Mech. 2019;64(2):281–305. doi:10.1007/s00466-019-01716-0.
37. Zhang L, Lu Y, Tang S, Liu WK. HiDeNN-TD: reduced-order hierarchical deep learning neural networks. Comput Methods Appl Mech Eng. 2022;389(39–41):114414. doi:10.1016/j.cma.2021.114414.
38. Lu Y, Li H, Saha S, Mojumder S, Al Amin A, Suarez D, et al. Reduced order machine learning finite element methods: concept, implementation, and future applications. Comput Model Eng Sci. 2021;129(3):1351–71. doi:10.32604/cmes.2021.017719.
39. Fish J, Yu Y. Data-physics driven reduced order homogenization. Int J Numer Meth Eng. 2023;124(7):1620–45. doi:10.1002/nme.7178.
40. Yu Y, Fish J. Data-physics driven reduced order homogenization for continuum damage mechanics at multiple scales. Int J Multiscale Computat Eng. 2024;22(1):1–14. doi:10.1615/IntJMultCompEng.2023049164.
41. Lefik M, Boso DP, Schrefler BA. Artificial Neural Networks in numerical modelling of composites. Comput Methods Appl Mech Eng. 2009;198(21–26):1785–804. doi:10.1016/j.cma.2008.12.036.
42. Liu Z, Wu CT, Koishi M. A deep material network for multiscale topology learning and accelerated nonlinear modeling of heterogeneous materials. Comput Meth Appl Mech Eng. 2019;345(4):1138–68. doi:10.1016/j.cma.2018.09.020.
43. Masrouri M, Qin Z. Towards data-efficient mechanical design of bicontinuous composites using generative AI. Theor Appl Mech Lett. 2024;14(1):100492. doi:10.1016/j.taml.2024.100492.
44. Oskay C, Fish J. Eigendeformation-based reduced order homogenization for failure analysis of heterogeneous materials. Comput Meth Appl Mech Eng. 2007;196(7):1216–43. doi:10.1016/j.cma.2006.08.015.
45. Yue J, Yuan Z. A study on equivalence of nonlinear energy dissipation between first-order computational homogenization (FOCH) and reduced-order homogenization (ROH) methods. Theor Appl Mech Lett. 2021;11(1):100225. doi:10.1016/j.taml.2021.100225.
46. Huang S, Yue J, Liu X, Ren P, Zu L, Yuan Z. A framework of defining constitutive model for fibrous composite material through reduced-order-homogenization method with analytical influence functions. Compos Struct. 2023;314(2):116968. doi:10.1016/j.compstruct.2023.116968.
47. Fish J, Filonova V, Yuan Z. Hybrid impotent-incompatible eigenstrain based homogenization. Int J Num Meth Eng. 2013;95(1):1–32. doi:10.1002/nme.4473.
48. Ma H, Gao XL. Strain gradient solution for a finite-domain Eshelby-type plane strain inclusion problem and Eshelby's tensor for a cylindrical inclusion in a finite elastic matrix. Int J Sol Struct. 2011;48(1):44–55. doi:10.1016/j.ijsolstr.2010.09.004.
49. Li S, Wang G, Sauer RA. The eshelby tensors in a finite spherical domain—part II: applications to homogenization. J Appl Mech, Transact ASME. 2007;74(4):784–97. doi:10.1115/1.2711228.
50. Li S, Sauer RA, Wang G. The eshelby tensors in a finite spherical domain—part I: theoretical formulations. J Appl Mech. 2007;74(4):770–83. doi:10.1115/1.2711227.
51. Li S, Wang G. Introduction to micromechanics and nanomechanics. 2nd ed. Singapore: World Scientific; 2017.
52. Fish J. Practical multiscaling. Hoboken, NJ, USA: John Wiley & Sons; 2013.